Journal of Hazardous Materials 488 (2025) 137374

Contents lists available at ScienceDirect

Journal of Hazardous Materials

journal homepage: www.elsevier.com/locate/jhazmat

Regulation of calcium signaling prevents neuronal death mediated by NIST DEP in xenoferroptotic cell death conditions

Leshan Zhang [a,1], Hong Yan [a,1], Mohammad Saidur Rahman [a], Christina HT J. Mol-van der Veen [a], Ana Manzano Covarrubias [a], Karim Rafie [a], Diana Pendin [c,d], Martina Schmidt [a,b,*,2], Amalia M. Dolga [a,e,*,3]

[a] Department of Molecular Pharmacology, Groningen Research Institute of Pharmacy, Faculty of Science and Engineering, University of Groningen, Groningen, The Netherlands
[b] Groningen Research Institute for Asthma and COPD (GRIAC), University of Groningen, University Medical Center Groningen, Groningen, the Netherlands
[c] Neuroscience Institute, Padua Section, National Research Council, Padua, Italy
[d] Department of Biomedical Sciences, University of Padua, Padua, Italy
[e] Depatment of Pathology and Medical Biology, University Medical Center of Groningen, Groningen, The Netherlands

HIGHLIGHTS

- NIST DEP aggravates RSL-3-induced ferroptotic cell death in neuronal cells.
- NIST DEP increases calcium levels in ferroptosis-sensitive cells.
- Calcium regulators alleviate ferroptosis accelerated by NIST DEP and RSL-3.
- NIST DEP contributes to xenoferroptotic cell death pathway.

GRAPHICAL ABSTRACT

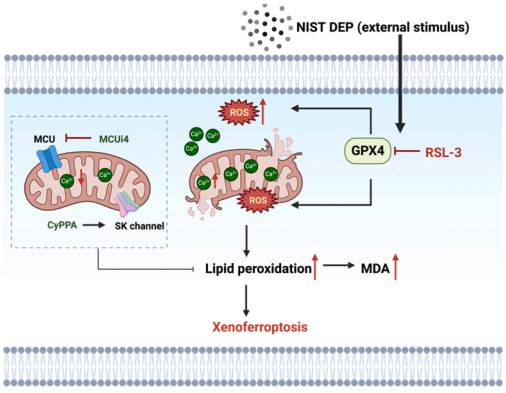

ARTICLE INFO

Keywords:
Diesel exhaust particle
Calcium
Mitochondria
Xenoferroptosis
Oxidative stress

ABSTRACT

Increased calcium levels are associated with the ferroptosis pathway in neurodegenerative conditions. Recent evidence showed that exposure to particulate matter (PM) could accelerate the pathology of neurodegenerative diseases. However, the molecular mechanisms of how PM could affect brain cell pathology is not fully understood. We hypothesized that diesel exhaust particles (NIST DEP) could alter the ferroptosis pathway through calcium signaling, and therefore accelerate the cell death pathway. In this study, we used mouse hippocampal neuronal-like HT22 cells to evaluate whether exposure to NIST DEP could accelerate RSL-3-induced ferroptosis

* Correspondence to: Antonius Deusinglaan 1, 9713 AV Groningen, the Netherlands.
E-mail addresses: m.schmidt@rug.nl (M. Schmidt), a.m.dolga@rug.nl (A.M. Dolga).
[1] These authors contributed equally to this work.
[2] https://orcid.org/0000-0003-3075-0630
[3] https://orcid.org/0000-0001-5400-5614

https://doi.org/10.1016/j.jhazmat.2025.137374
Received 24 November 2024; Received in revised form 3 January 2025; Accepted 23 January 2025
Available online 25 January 2025

by increasing calcium deregulation, mitochondrial dysfunction and reactive oxygen species (ROS). MTT assay results showed that NIST DEP (25, 50, 75, and 100 μg/mL) did not significantly reduce the survival rate of HT22 cells, while NIST DEP significantly increased RSL-3-induced ferroptotic cell death in a concentration-dependent manner. Based on fluorescence image analysis, co-exposure to NIST DEP and RSL-3 disrupted HT22 cell mitochondrial morphology, intracellular and mitochondrial calcium levels. Combined exposure resulted in an increase in ER-mitochondria contact sites measured by proximity ligation assay (PLA) compared to control solvent group. Additionally, lipid peroxidation, mitochondrial ROS and malondialdehyde content, were increased significantly by combined exposure to NIST DEP and RSL-3. Interestingly, the calcium regulators of the mitochondrial calcium uniporter MCUi4 and positive modulation of small conductance calcium-activated potassium channels by CyPPA significantly preserved cellular metabolic activity, restored calcium homeostasis, and alleviated fragmentation of mitochondria. Consequently, targeting calcium signaling may be promising therapeutic option for xenoferroptotic conditions in which PM affect cell survival.

1. Introduction

The second messenger calcium participates in a variety of physiological processes including neurotransmission, mitochondrial function and energy metabolism [1,2]. The small conductance calcium-activated potassium (SK) channels are essential regulators of intracellular calcium pathways [3–5]. The SK channels open upon alterations in intracellular calcium levels, regulate neuronal excitability, firing pattern and are involved in the after-hyperpolarization process [6–9]. The SK channels have been shown to elicit neuroprotective effects in various cell death conditions, by regulating calcium signaling and mitochondrial function [8–11]. Mitochondria are important sites for the production of intracellular reactive oxygen species (ROS), and play a key role in maintaining cellular calcium homeostasis and metabolic regulation [12]. Mitochondrial calcium uniporter (MCU) is a protein channel located in the inner membrane of the mitochondria, responsible for transporting calcium from the cytoplasm into the mitochondria [13,14]. Therefore, the opening and closing of MCU channels can regulate calcium levels within mitochondria [15].

Ferroptosis is a form of cell death associated with the progression of neurodegenerative diseases. Although the main driving factors of ferroptosis are iron metabolism and lipid peroxidation, calcium deregulation also plays a certain role in the process of ferroptosis [16–19]. Early dysregulation of cellular redox status observed in ferroptosis may perturb Ca^{2+} homeostasis and signaling, promoting neuronal ferroptosis [20].

Ferroptosis has been reported to be involved in the pathology of neurodegenerative diseases [21]. Neurodegenerative diseases, such as Alzheimer's disease (AD), Parkinson's disease (PD), and amyotrophic lateral sclerosis (ALS) are characterized by gradual loss of neuronal cells, resulting in a decline in patients' cognitive, motor, and sensory functions [22]. Environmental factors, such as air pollution have attracted attention as they can contribute to the pathology of neurodegenerative diseases [23]. Epidemiological studies, and recent *in vivo* evidence indicated the presence of particulate matter (PM) in the brain, especially fine particles with a diameter of less than 2.5 μm [24–30]. The latest data from the World Health Organization (WHO) showed that more than 99 % of people worldwide are exposed to air pollution to levels exceeding the recommended guidelines [31]. Long-term exposure to pollutants can increase the risk of respiratory, central nervous system (CNS) and cardiovascular-related diseases and mortality. Molecular pathways involved in these conditions include mitochondrial damage, neuroinflammation and oxidative stress [32]. The adverse effects of PM2.5 exposure to the nervous system may indirectly accelerate the pathological process of ferroptosis through calcium ion imbalance and excessive ROS [33]. Indeed, carbon-based nanoparticle exposure induced ferroptosis and inflammation in microglial BV2 cells by ROS accumulation and increasing cytoplasmic calcium levels [34]. However, the mechanisms underlying NIST DEP-accelerated ferroptosis and the calcium pathway represent a largely neglected research area.

In this study, we aimed to explore the effects of NIST DEP on RSL-3-induced ferroptosis and to further investigate the underlying mechanisms associated with calcium deregulation. Our findings revealed that NIST DEP aggravated RSL-3-induced ferroptotic cell death. Furthermore, we demonstrated that administration of calcium regulators MCUi4 and CyPPA rescued the impaired cellular metabolic activity caused by co-treatment of RSL-3 and NIST DEP in HT22 cells, and simultaneously modulated intracellular and mitochondrial calcium homeostasis, improved mitochondrial morphology, and reduced lipid peroxidation. These findings indicate RSL-3-induced ferroptosis aggravated by NIST DEP involves calcium imbalance.

2. Materials and methods

2.1. NIST DEP preparation

NIST DEP are diesel exhaust particles (DEP) 2975 obtained from the National Institute of Sciences and Technology (NIST, USA). NIST DEP was added to phosphate buffer solution (PBS) buffer to achieve a final particle suspension concentration of 2.5 mg/mL. Subsequently, the suspension was sonicated for 30 min in a water bath (#06524, Branson 2510; Gemini b.v., the Netherlands), followed by probe sonication (Ultrasonic Processor, Sonics Vibra Cell, the Netherlands) for 30 sec on ice bath to avoid excessive heat generation. Tween 80 (0.1 % v/v) (#9005–65–6; Sigma-Aldrich, the Netherlands) was added to achieve an even and stable particle suspension. PBS supplemented with Tween 80 (0.1 % v/v) was used as control solvent group. Finally, the NIST DEP solution was stored at 4°C before use in each experiment [35].

2.2. Cell culture and treatment

The mouse hippocampal neuronal cell line HT22 (kindly provided by Prof. Carsten Culmsee) was used as cell model [36]. Cell culturing was performed as described in detail before [37]. Briefly, cells were cultured in Dulbecco's Modified Eagle Medium (DMEM, #42430025, Gibco, Thermo Fisher Scientific, the Netherlands) supplemented with 10 % fetal bovine serum (FBS; Hyclone, USA), 1 % Sodium Pyruvate (#11360070, 100 mM, Gibco, Thermo Fisher Scientific, the Netherlands), 2 % penicillin and streptomycin ((#15070063, 5×10^3 U/mL, Gibco, Thermo Fisher Scientific, the Netherlands) at 37°C in a humidified incubator with 5 % CO_2. Cells were passaged every other day by trypsinization (Trypsin-EDTA at 0.20 %) at a 1:3 dilution. The NIST DEP concentrations used in this study correspond to real-life environmental exposure levels, with studies calculating that 1–100 μg/mL DEP concentrations correspond to 1.4–143 μg/mL particle doses. Based on considerations of the culture surface area, this concentration range was coordinated to a particle dose/area of 0.2–20 μg/cm^2 [38]. In addition, the highest concentration range used in previous studies of PM-induced brain damage was 100–400 μg/mL [39–41]. Therefore, we selected concentrations of 25, 50, 75, and 100 μg/mL to ensure environmental relevance and consistency with existing studies. Ferroptosis inducer RSL-3 (#S8155, Selleckchem, USA), specific ferroptosis inhibitor Ferrostatin-1 (Fer-1; #SML0583, Sigma-Aldrich, Germany), apoptosis inhibitor QVD (#1135695–98–5, MP Biomedicine, USA), mitochondrial

calcium uniporter (MCU) inhibitor MCUi4 (#7195, Tocris bioscience, UK) and small conductance calcium-activated potassium (SK) channel activator CyPPA (#73029–73–9, Tocris bioscience, UK) were added to HT22 cells for co-treatment. In subsequent co-exposures, NIST DEP was used at a concentration of 100 μg/mL. The treatment time of HT22 cells related to Ca^{2+}, lipid peroxidation, MDA, mitochondrial ROS (MitoROS) and proximity ligation assay (PLA) experiments was about 6 hrs, during which time potential cell morphology change can be observed due to different treatments. The treatment time of all other experiments was 17 hrs.

2.3. Cell metabolism assay

To determine the effects of NIST DEP and RSL-3 used either alone or in combination on cell viability, HT22 cells were seeded into 96-well plates at a seeding density of 9×10^3 cells per well. After 17–18 hrs of treatment, 3-(4,5-Dimethyl-2-thiazolyl)-2,5-diphenyl-2H-tetrazolium bromide (MTT) working solution at a concentration of 0.5 mg/mL was added to each well, and 96-well plates were left in the cell incubator (37°C, 5 % CO_2) for 1 hr. Then, the MTT working solution was removed, and the 96-well plate was inverted and lightly patted to allow sufficient removal of the residual fluid. After 1 hr of freezing at −20°C, the formazan product was dissolved in 70 μL dimethyl sulfoxide (DMSO) (#D8418, Lot#SHBH9942; Sigma-Aldrich, Germany). Thereafter, the mixture was shaken at room temperature for 45 min in the dark, absorbance was read using Synergy H1 Multi-Mode reader (Biotek, LA, USA) at wavelengths of 570 nm and 630 nm [42].

2.4. Cell death assay

Cell death assay was determined by PI/Hoechst 33342 fluorescent staining. HT22 cells were cultured in ibidi plate (#80826, ibidi GmbH) at 20×10^3 cells per well and cultured 24 hrs before treatment. After exposure to NIST DEP, RSL-3, Fer-1, calcium regulators MCUi4 and CyPPA alone or in combination, Hoechst 33258 (#H3570; Invitrogen, the Netherlands) at a final concentration of 1 μg/mL and 3 μM propidium iodide (PI; #V13242; Fisher Scientific, Landsmeer, the Netherlands) were added to each well for 10 min in the dark [43]. Ten images were taken under a Nikon Inverted Fluorescence Microscope ECLIPSE Ti2 at 40X magnification for each condition. The ratio of PI-positive cells to total cells was quantified using ImageJ software.

2.5. Calcium measurements

The intracellular calcium level was measured by Fluo4-AM (# F14201; Invitrogen, the Netherlands). HT22 cells were seeded in ibidi plate (20×10^3 cells/well) and after exposure to NIST DEP and RSL-3 alone and in combination with or without the calcium regulators MCUi4 and CyPPA, Hanks' balanced salt solution (HBSS, pH 7.2) (#14065–056; Gibco, Thermo Fisher Scientific, the Netherlands) was added to remove the remaining treatment solution in each well. Then, cells were incubated with 2.5 μM Fluo-4 AM/Hoechst33342 for 15 min at 37°C in the dark [42]. After removing the dye, HBSS buffer was added again before imaging. Fluorescence was measured at Ex/Em = 494/516 nm. Ten images were taken under a Nikon Inverted Fluorescence Microscope ECLIPSE Ti2 at 20X magnification for each condition. Mean fluorescence intensity of Fluo4-AM was quantified using ImageJ software.

The mitochondrial calcium level was measured by Rhod-2 AM (#R1244; Invitrogen, the Netherlands) or with a modified version of ratiometric dye Mt-fura-2 [44,45]. The ratiometric properties of the latter ensure accurate measurement of mitochondrial Ca^{2+} levels [45]. Cells were incubated with 2 μM Rhod-2 AM/Hoechst33342 or 1 μM Mt-fura-2 AM for 15 min at 37°C in the dark. AM versions of both probes are hydrolyzed by cellular esterases, generating the functional version of the probe which binds calcium in the mitochondrial matrix [46]. After removing the fluorescence dye, HBSS buffer was added before imaging. Fluorescence was measured at Ex/Em = 552/581 nm (Rhod2-AM) or Ex/Em = 340, 380/510 nm (Mt-fura-2). Ten images were taken under a Nikon Inverted Fluorescence Microscope ECLIPSE Ti2 at 20X magnification for each condition. Mean fluorescence intensity of Rhod2 and mean fluorescence ratio of Mt-fura-2 (Fura340/Fura380 Ratio = mean fluorescence at 340/mean fluorescence at 380 nm) were quantified using ImageJ software.

2.6. Proximity ligation in situ assay

HT22 cells were seeded in 24-well plates with coverslips (35×10^3 cells/well). After treatment for 6 hrs, the cells were fixed with 4 % paraformaldehyde (PFA) for 30 min at room temperature and permeabilized with 0.1 % Triton X-100 for 30 min [37]. After washing three times with PBS, the coverslips were removed and incubated in a humidity chamber with blocking solution at 37°C for 1 hr. Then, primary antibodies IP3R (1:4000) (ab5804, Abcam, UK) and VDAC1(1:800) (ab14734, Abcam, UK) were added and incubated overnight at 4°C. After the coverslips were washed twice, the corresponding secondary antibodies PLA probe plus (Anti-Rabbit, DUO92002, Sigma-Aldrich, Germany) and minus (Anti-Mouse, DUO92004, Sigma-Aldrich, Germany) coupled to DNA oligonucleotides were added. The principle of the PLA assay is based on the fact that the distance between two proteins is less than 40 nm, so that the addition of ligation buffer can form a closed-circle DNA template. Then amplification buffer was added and incubated at 37°C for 100 min. The coverslips were fixed on the glass slides after adding PLA counting culture medium containing DAPI for 15 min. Images were taken under a confocal microscope Zeiss CellDiscoverer7 (Zeiss, Germany) at Ex/Em = 594/624 nm and quantified using imageJ software.

2.7. Mitochondrial imaging

The mitochondrial morphology of cells was determined using Mitotracker Deep Red (#22426, Fisher Scientific, the Netherlands) [42]. HT22 cells (25×10^3 cells/well) were seeded in removable 8-well ibidi plates. After overnight exposure to NIST DEP and RSL-3 alone and in combination with or without the calcium regulators MCUi4 and CyPPA, Mitotracker Deep Red was added to each well at a final concentration of 100 nM for 30 min at 37°C in the dark. Before fixing the cells with 4 % PFA at room temperature, cells were washed with prewarmed PBS. After fixation for 15 min, cells were washed three times with PBS. Then, a coverslip with DAPI was used to cover the cells. Images were taken under a Nikon Inverted Fluorescence Microscope ECLIPSE Ti2 and quantified using imageJ software.

The mitochondrial footprint was analyzed based on the skeleton diagram using the MiNA plugin for Fiji (https://github.com/ScienceToolkit/MiNA) [47]. MiNA provides a simplified analysis method for two-dimensional mitochondrial morphologies, including dots, rods, and branched networks. Fifteen single cells were analyzed in each group.

The mitochondrial branch length and mitochondrial branch perimeter were measured using the *Mitochondria Analyzer* plugin (https://github.com/AhsenChaudhry/ Mitochondria-Analyzer) provided by imageJ software [48]. The optimal threshold condition of the image was first determined, and then a uniform threshold was maintained for subsequent analysis and measurement. Ten images per group were analyzed, and the experiment was repeated at least three times with different cell passage numbers.

2.8. Lipid ROS detection

The lipid ROS was determined using BODIPY 581/591 C11 (#D3861, Fisher Scientific, Landsmeer, the Netherlands) [49,50]. HT22 cells were seeded in 8-well ibidi plate (20×10^3 cells/well). After 6 hrs of different treatments, BODIPY 581/591 C11 and Hoechst 33258 dye

were added to each well at final concentrations of 2 μM and 1 μg/mL, respectively. After incubation at 37°C in the dark for 30 min, images were taken under a Nikon Inverted Fluorescence Microscope ECLIPSE Ti2 and quantified using imageJ software.

2.9. Malondialdehyde assay

Thiobarbituric acid reactive substances (TBARS) were used to measure the MDA level as a breakdown product of the terminal stage of polyunsaturated fatty acid peroxidation [51]. HT22 cells were seeded in 6-well plates (25×10^4 cells/well). The plate was kept on ice after NIST DEP and RSL-3 alone and in combination with or without the calcium regulators MCUi4 (5 μM) and CyPPA (10 μM) exposure and then washed with ice-cold PBS before harvesting the cells with ice-cold ultra-pure water. The collected cells were sonicated for 5 sec and freeze-thawed, and this procedure was repeated three times. The cell lysates were mixed with 10 % trichloroacetic acid and incubated on ice for 15 min before centrifugation at 5000xg for 15 min at 4°C. After that, the supernatant was mixed with 0.75 % thiobarbituric acid and added to the PCR tube. Then, the PCR instrument was set up with a program (heating at 95°C for 30 min and cooling to 20°C) and the fluorescence was measured at Ex/Em = 540/590 nm.

2.10. Mitochondrial oxidation assay

Mitochondrial ROS was measured by microplate reader and fluorescence microscopy using MitoSOX red (#36008, Fisher Scientific, the Netherlands). For these two assay procedures, HT22 cells were seeded in black 96-well plate (9×10^3 cells/well) and 8-well ibidi plate (20×10^3 cells/well) in preparation for microplate reader and fluorescence microscopy imaging, respectively. After 6 hrs exposure to NIST DEP and RSL-3 alone and in combination with or without the calcium regulators MCUi4 (5 μM) and CyPPA (10 μM), MitoSOX Red dye was added to each well at a final concentration of 1.25 μM. The cells were then incubated at 37°C, 5 % CO_2 environment in the dark. After 30 min, the dye was removed and pre-warmed PBS was added. Finally, the 96-well plate was read using a microplate reader at Ex/Em = 510/580 nm, and the 8-well ibidi plate was imaged using a Nikon Inverted Fluorescence Microscope ECLIPSE Ti2 under the same wavelength conditions.

2.11. Statistical analysis

All data are presented as mean ± standard deviation (SD) unless otherwise specified. Statistical analysis was performed using one-way analysis of variance (ANOVA) and Tukey's post hoc multiple comparison test. $^{*}p < 0.05$, $^{**}p < 0.01$, $^{***}p < 0.001$, $^{****}p < 0.0001$. Data were analyzed and plotted using GraphPad Prism version 8 (USA).

3. Results

3.1. NIST DEP increases HT22 ferroptotic cell death induced by RSL-3

To determine the potential cell toxicity effects of NIST DEP on HT22 cells, four different concentrations of NIST DEP (25, 50, 75, 100 μg/mL) were used. As shown in the bright field image (Fig. 1A), no morphological changes were observed at the highest concentration of NIST DEP compared to the control solvent group. In agreement with the lack of effect on cell morphology, we did not observe significant changes in cell metabolic activity even with the highest tested concentration of NIST DEP (100 μg/mL), as measured by an MTT assay (Fig. 1B).

Next, we tested various concentrations for induction of ferroptotic cell death with a well-known ferroptosis inducer, ras selective lethal small molecule 3 [(1 S,3 R)-RSL-3] [52] (Fig. S1). RSL3 (50–400 nM) (Fig. 2A) induced a concentration-dependent cell death in HT22 cells. As RSL-3 induced more than 50 % cell death at concentrations higher than 150 nM, we used a concentration of 150 nM in the following experiments to have less than 50 % cell death. This concentration of RSL-3 allowed testing whether NIST DEP can affect cell survival in cells sensitized to ferroptosis and have cell death rates below 50 % (Fig. 1B). RSL-3 (150 nM) induced a slight cell morphological change such as shrinkage and spotting in some cells, and sensitized cells to ferroptotic cell death (25.5 ± 4.9 %). Combined exposure to NIST DEP and RSL-3 led to even more profound widespread cell morphological alteration, with almost all cells becoming dot-like and fragmented (Fig. 1A). Cell metabolic activity measurements revealed that combined exposure to different concentrations of NIST DEP (25, 50, 75, 100 μg/mL) and RSL-3 (150 nM) led to a decrease in the cell viability in a NIST DEP concentration-dependent manner (Fig. 1B). We also measured other ferroptosis inducers, Erastin and Glutamate, and observed similar effects in the NIST DEP combination group (Fig. S2). We applied 100 μg/mL NIST DEP for the following experiments.

As MTT assay is related to cell metabolic activity and indirectly to cell viability, we tested the effect of the combined exposure NIST DEP and RSL-3 on the nuclei integrity by performing PI/Hoechst 33258 double staining.

This combined exposure led to a significant increase in PI uptake, as vizualized by the microscopy images (Fig. 1C) and their corresponding quantification (81.8 ± 8.3 %) (Fig. 1D). To determine whether the type of the cell death caused by the co-exposure of NIST DEP and RSL-3 cells was related to ferroptosis, we treated cells with the ferroptosis inhibitor ferrostatin-1 (Fer-1) in the presence of the combined cell exposure to NIST DEP and RSL-3. In the NIST DEP or Fer-1 alone treatment groups, PI-positive cells were barely observed by the fluorescence microscopy. As shown in Fig. 1C, the number of PI-positive cells in RSL-3 alone-treated group (11.8 ± 4.4 %) was higher than that in the control group (3.8 ± 2.6 %). However, when NIST DEP was added together with RSL-3, the percentage of dead cells further increased to 81.8 ± 8.3 % from 11.8 ± 4.4 % in RSL-3 treatment (Fig. 1D). In contrast, the increased PI-positive cells caused by RSL-3 treatment (11.8 ± 4.4 %) or combined RSL-3 and NIST DEP (81.8 ± 8.3 %) were nearly completely reduced by Fer-1 treatment to 2.1 ± 1.0 % and 4.8 ± 2.6 % (Fig. 1D). Moreover, Fer-1 significantly completely abolished the impact of co-treatment on cell viability from 82.5 ± 5.9 % to 29.0 ± 4.4 %, whereas the apoptosis inhibitor QVD (31.4 ± 2.0 %) showed no effects on the cell death induced by RSL-3 and NIST DEP (29.0 ± 4.4 %) (Fig. 1E). These results suggested that the acceleration of cell death caused by NIST DEP exposure involves ferroptosis rather than apoptosis.

3.2. Combined exposure to NIST DEP and RSL-3 increases intracellular calcium levels

Increased intracellular calcium release has been shown to lead to ferroptosis [53]. Recent studies in our lab showed that the reduction of mitochondrial calcium uptake prevented ferroptosis [42]. Therefore, we assessed whether the regulation of mitochondrial calcium would impact cell damage induced by NIST DEP in sensitized cells to ferroptosis. To modulate calcium signals we used the MCU inhibitor, MCUi4 and the SK channel activator, CyPPA. Fluo4-AM fluorescent dye was used to measure intracellular calcium levels. Consistent with the fluorescence images (Fig. 2A), quantification of the fluorescence intensity of Fluo4-AM showed a slight increase in the calcium signals in the presence of NIST DEP by 1.1 ± 0.1 - fold. RSL-3 treatment increased the fluorescence intensity by 1.2 ± 0.1 -fold compared with the control group. The combined exposure led to an increase of 1.5 ± 0.2 - fold. MCUi4 or CyPPA reduced the intracellular calcium level that was elevated in response to the combined exposure with NIST DEP and RSL-3. The fluorescence intensity of Fluo4-AM decreased to 1.0 ± 0.03 - fold and 1.1 ± 0.03 - fold following treatment with MCUi4 and CyPPA, respectively (Fig. 2B). These results suggested that co-treatment with NIST DEP and RSL-3 may lead to an increase in intracellular calcium levels.

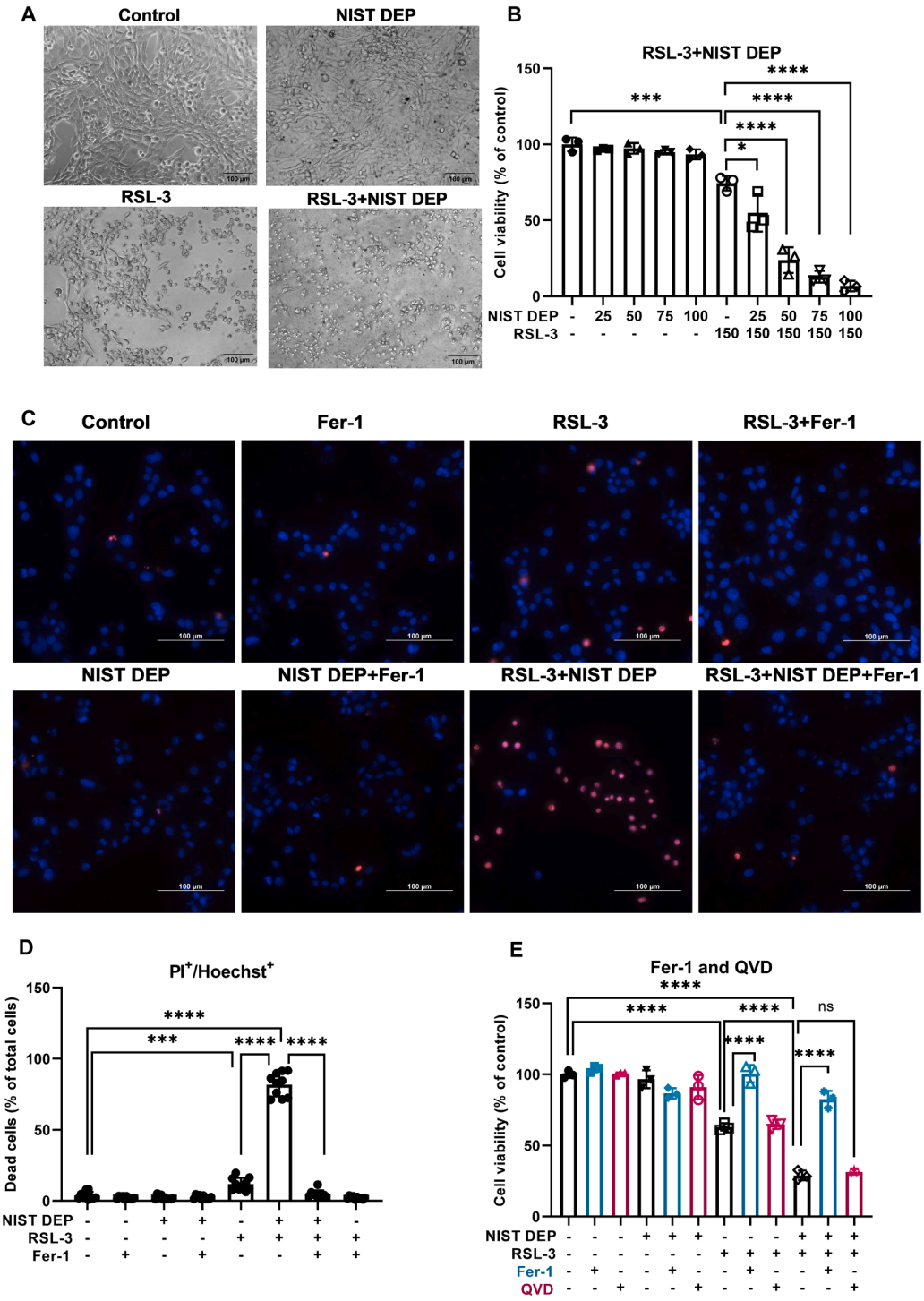

Fig. 1. NIST DEP increases RSL-3-induced HT22 ferroptotic cell death. (A) Brightfield images of HT22 cells treated with NIST DEP (100 μg/mL), RSL-3 (150 nM), and combined RSL-3 and DEP (scale bar = 100 μm). (B) MTT assay for the metabolic activity of HT22 cells following treatment with different concentrations of NIST DEP alone (25–100 μg/mL) or in combination with RSL-3 (150 nM). The cell viability of the control (solvent-treated) group was defined as 100 %. (C) PI/Hoechst 33342 double-stained fluorescence images at 40x magnification after 17 hrs exposure to NIST DEP, RSL-3, Fer-1 (5 μM) alone or in combination. Red: dead cells, Blue: nucleus (scale bar =100 μm). (D) Quantitative analysis of PI-positive cells was performed based on 10 fluorescent images per condition (mean ± SD). The percentage of total cells in the control group was defined as 100 %. (E) MTT assay for the viability of HT22 cells following 17 hrs exposure to NIST DEP, RSL-3, ferroptosis inhibitor Fer-1 (5 μM) and apoptosis inhibitor QVD (10 μM) alone or in combination. Each condition had 5–6 technical replicates. The cell viability of the control group was defined as 100 %. Statistical analysis was performed using one-way ANOVA followed by Tukey's post hoc multiple comparison test. $^{*}p < 0.05$, $^{***}p < 0.001$, $^{****}p < 0.0001$, no significant (ns). All experiments were repeated at least three times as biological replicates.

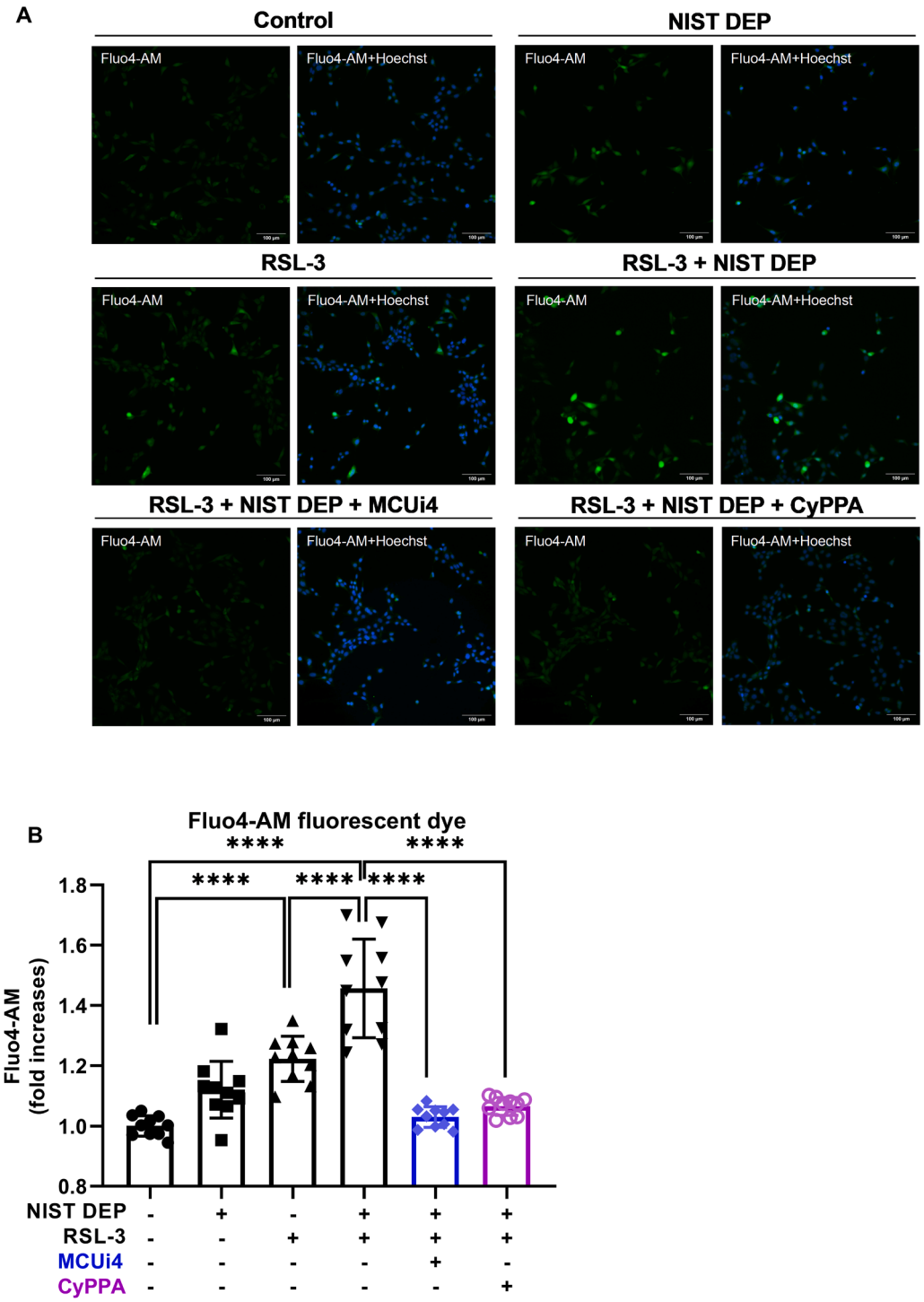

Fig. 2. Intracellular calcium levels are increased by NIST DEP and RSL-3 co-treatment. (A) Fluo4-AM fluorescence images at 20x magnification after 6 hrs exposure to NIST DEP and RSL-3 alone and in combination with or without the calcium regulators MCUi4 (5 μM) and CyPPA (10 μM). Green: Fluo4-AM positive cells, Blue: nucleus (scale bar =100 μm). (B) Quantitative analysis of Fluo4-AM positive cells was performed based on 10 fluorescent images per condition (mean ± SD). Statistical analysis was performed using one-way ANOVA followed by Tukey's post hoc multiple comparison test. $^{****}p < 0.0001$. All experiments were repeated at least three times as biological replicates.

3.3. Combined exposure to NIST DEP and RSL-3 increases the number of mitochondrial-ER contact sites

To elucidate the sources of intracellular calcium in response to air particles in conditions of ferroptosis-sensitized cells, we evaluated the interaction between IP3R in the ER and VDAC1 in the mitochondria by a PLA assay [54]. The number of red PLA signal sites following NIST DEP and RSL-3 exposure was significantly higher than that in the control (solvent) group, while the addition of MCUi4 and CyPPA significantly reduced ER-mitochondria contact sites (Fig. 3A). As the quantitative analysis is shown in Fig. 3B, the number of single-cell PLA signal sites in cells exposed to NIST DEP and RSL-3 increased to 99 ± 41 compared with 43 ± 18 in the control cells. However, both MCUi4 and CyPPA significantly decreased single-cell PLA signal sites to 42 ± 18 and 32

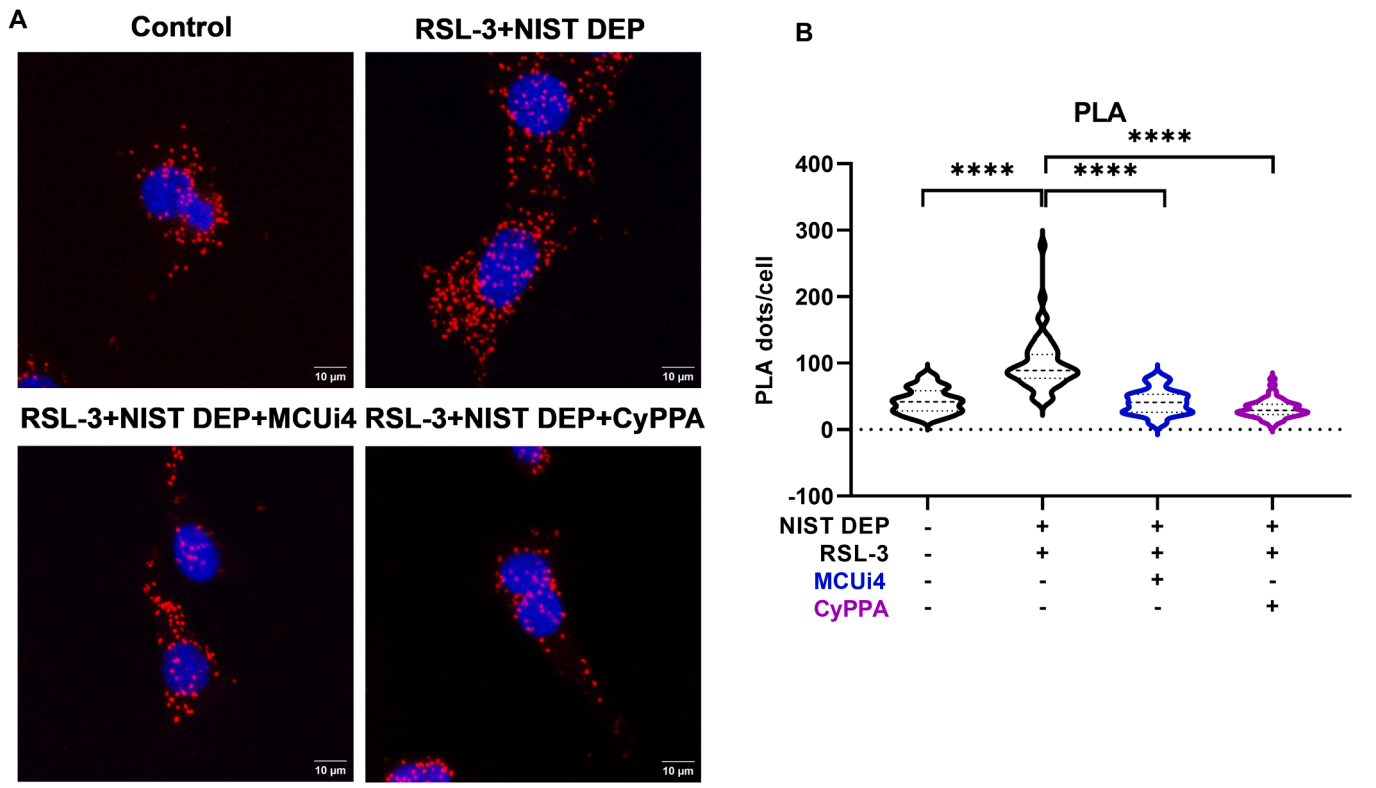

Fig. 3. ER-mitochondria contact sites are increased by NIST DEP and RSL-3 co-treatment. (A) PLA fluorescence images at 40x magnification after 6 hrs exposure to NIST DEP and RSL-3 with or without the calcium regulators MCUi4 (5 μM) and CyPPA (10 μM). Red: PLA dots, Blue: nucleus (scale bar = 10 μm). (B) Quantification of PLA dots from 50 single cells based on fluorescence images for each condition. Statistical analysis was performed using one-way ANOVA followed by Tukey's post hoc multiple comparison test. $^{****}p < 0.0001$. All experiments were repeated at least three times as biological replicates.

± 14, respectively. These results suggested that NIST DEP could induce an increase in mitochondrial calcium in ferroptotic-sensitized cells in response to an increase in the number of ER-mitochondrial contact sites.

3.4. Combined exposure to NIST DEP and RSL-3 increases mitochondrial calcium level

Next, we tested whether increased ER-mitochondrial contact sites mediated by NIST DEP in ferroptosis-sentisized cells could lead to increased mitochondrial calcium, and used Rhod2-AM as a fluorescent probe for mitochondrial calcium [44,55]. As shown in Fig. S3A, the red fluorescence signal of the RSL-3-treated cells was higher than that of the control group, and the addition of NIST DEP further increased the signal intensity of Rhod2-AM. Interestingly, the addition of calcium regulators MCUi4 and CyPPA attenuated the signal caused by the addition of NIST DEP. The quantification of mean fluorescence intensity of Rhod2-AM reported in Fig. S3B confirmed that mitochondrial calcium levels were significantly increased upon exposure to NIST DEP and RSL-3 (1.24 ± 0.04 - fold) compared with RSL-3 alone treatment cells (1.11 ± 0.03 - fold). The addition of both MCUi4 and CyPPA reduced the signal of Rhod2-AM from 1.24 ± 0.04 - fold in the co-treatment group to 1.04 ± 0.01 - fold and 1.06 ± 0.02 - fold, respectively.

The results were validated using Mt-fura-2, a novel ratiometric dye which is not affected by loading or motion artifacts [44], thus providing better insight into mitochondrial calcium levels. In Fig. 4A, fluorescence images recorded upon excitation at 340 nm (Fura340) and 380 nm (Fura380) are shown separately and then as a pseudo-color image representing the ratio of the two. The calculated ratio provides an estimation of mitochondrial calcium concentration. After 6 hours of RSL-3 challenge, a modest increase in Mt-fura-2 ratio was observed (0.80 ± 0.03), that was further increased in cells exposed to both NIST DEP and RSL-3 (0.92 ± 0.03).

Importantly, addition of MCUi4 or CyPPA decreased the Mt-fura-2 ratio to 0.86 ± 0.02 and 0.77 ± 0.03, respectively, compared with 0.92 ± 0.03 in the co-treatment group. (Fig. 4B) (Fig. 4C). Altogether, measurements performed with both Rhod2-AM and Mt-fura-2 AM fluorescent dyes indicated that co-treatment with NIST DEP and RSL-3 induced an increase in mitochondrial calcium levels.

3.5. Ferroptotic cell death induced by RSL-3 and NIST DEP is alleviated by the inhibition of mitochondrial calcium uniporter complex

We provided here evidence that exposure to NIST DEP in ferroptosis-sensitized cells led to increased intracellular calcium levels, ER-mitochondrial contact sites and mitochondrial calcium uptake. These processes could be prevented by inhibition of mitochondrial calcium uniporter complex with MCUi4 and activation of SK channels with CyPPA. Therefore, next we investigated whether these compounds could also prevent ferroptotic cell death in cells exposed to both NIST DEP and RSL-3, by PI/Hoechst 33258 double staining and a metabolic MTT assay. RSL-3 reduced the number of viable HT22 cells, and the addition of NIST DEP further increased cell death, as detected by PI analysis (Figs. 5A, 5B). However, the addition of MCUi4 or CyPPA protected against ferroptotic cell death induced by RSL-3 and NIST DEP co-treatment from 21.0 ± 6.6 % to 5.3 ± 2.8 % in case of MCUi4 and to 5.0 ± 2.2 % in case of CyPPA, respectively (Fig. 5B). Moreover, the PI analysis was paralleled by an MTT assay and showed that both CyPPA and MCUi4 significantly inhibited the NIST DEP and RSL-3-induced ferroptotic cell death. The cell metabolic activity increased from 43.8 ± 1.0 in the co-treatment group to 76.9 ± 3.6 in the CyPPA group and 91.1 ± 4.0 in the MCUi4 group. (Fig. 5C). These results indicated that ferroptosis induced by NIST DEP and RSL-3 co-treatment may be related to calcium deregulation.

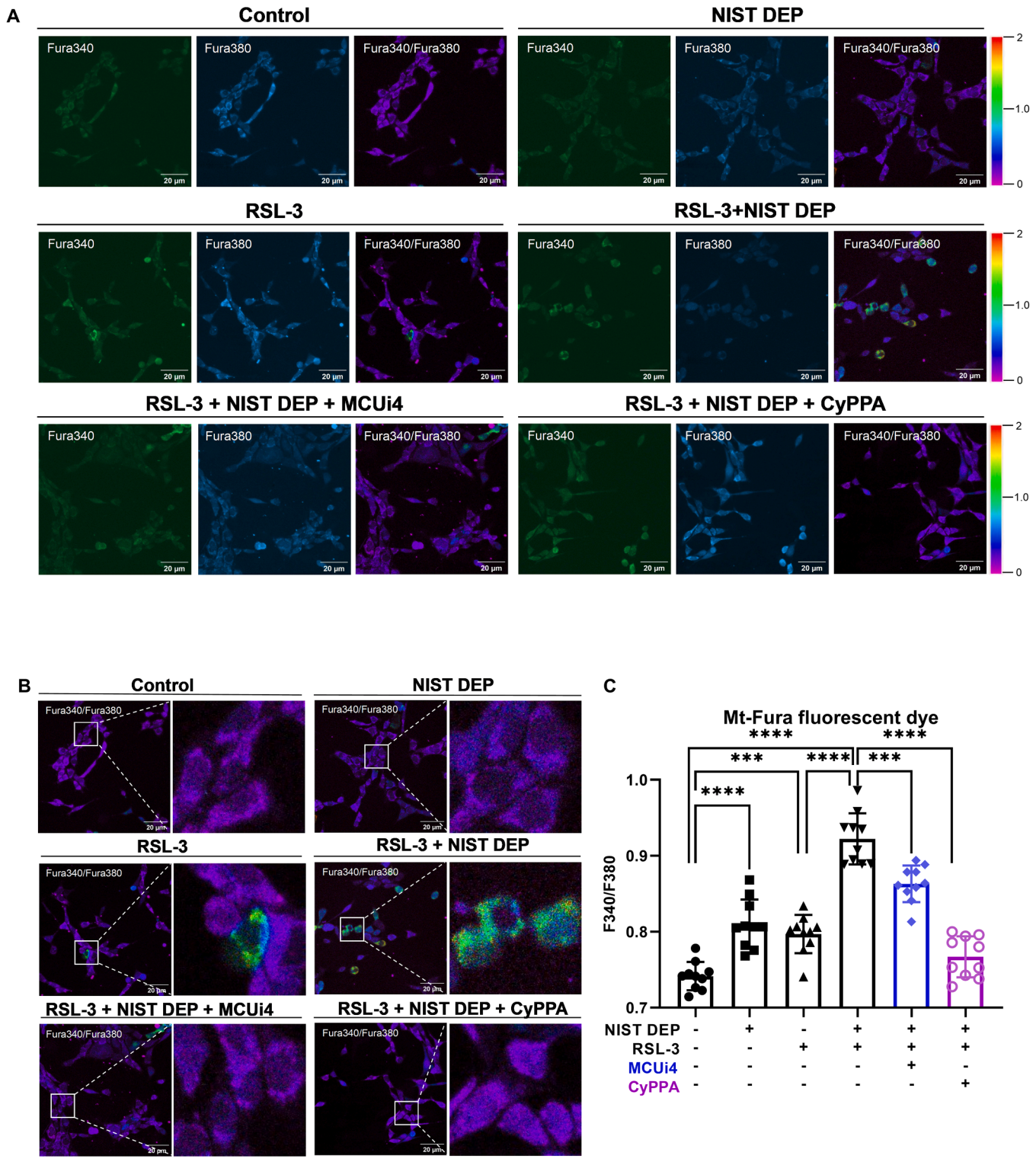

Fig. 4. Mitochondrial calcium levels are increased by NIST DEP and RSL-3 co-treatment. (A) Mt-fura-2 fluorescence images at 20x magnification after 6 hrs exposure to NIST DEP and RSL-3 alone and in combination with or without the calcium regulators MCUi4 (5 μM) and CyPPA (10 μM). Green: Fura 340, Blue: Fura 380 (scale bar = 20 μm). The ratio of fluorescence measured upon excitation at 340/380 nm (F340/F380) is shown in the right panel, ratio range from 0 to 2. (B) Fura340/Fura380 ratio picture of different treatments. Enlarged images of the boxed area were shown in the right panels. (C) Quantitative analysis of F340/F380 was performed based on 10 fluorescent images per condition (mean ± SD). Statistical analysis was performed using one-way ANOVA followed by Tukey's post hoc multiple comparison test. $^{***}p < 0.001$, $^{****}p < 0.0001$. All experiments were repeated at least three times as biological replicates.

3.6. Mitochondrial morphological alterations induced by RSL-3 and NIST DEP are prevented by mitochondrial calcium uniporter complex inhibition

Mitochondria not only played an important role in the regulation of calcium signaling, but a growing body of research suggested that mitochondrial damage was one of the most common hallmarks of neurodegeneration [12]. To explore the potential effect of NIST DEP on mitochondrial morphology, we studied whether mitochondrial

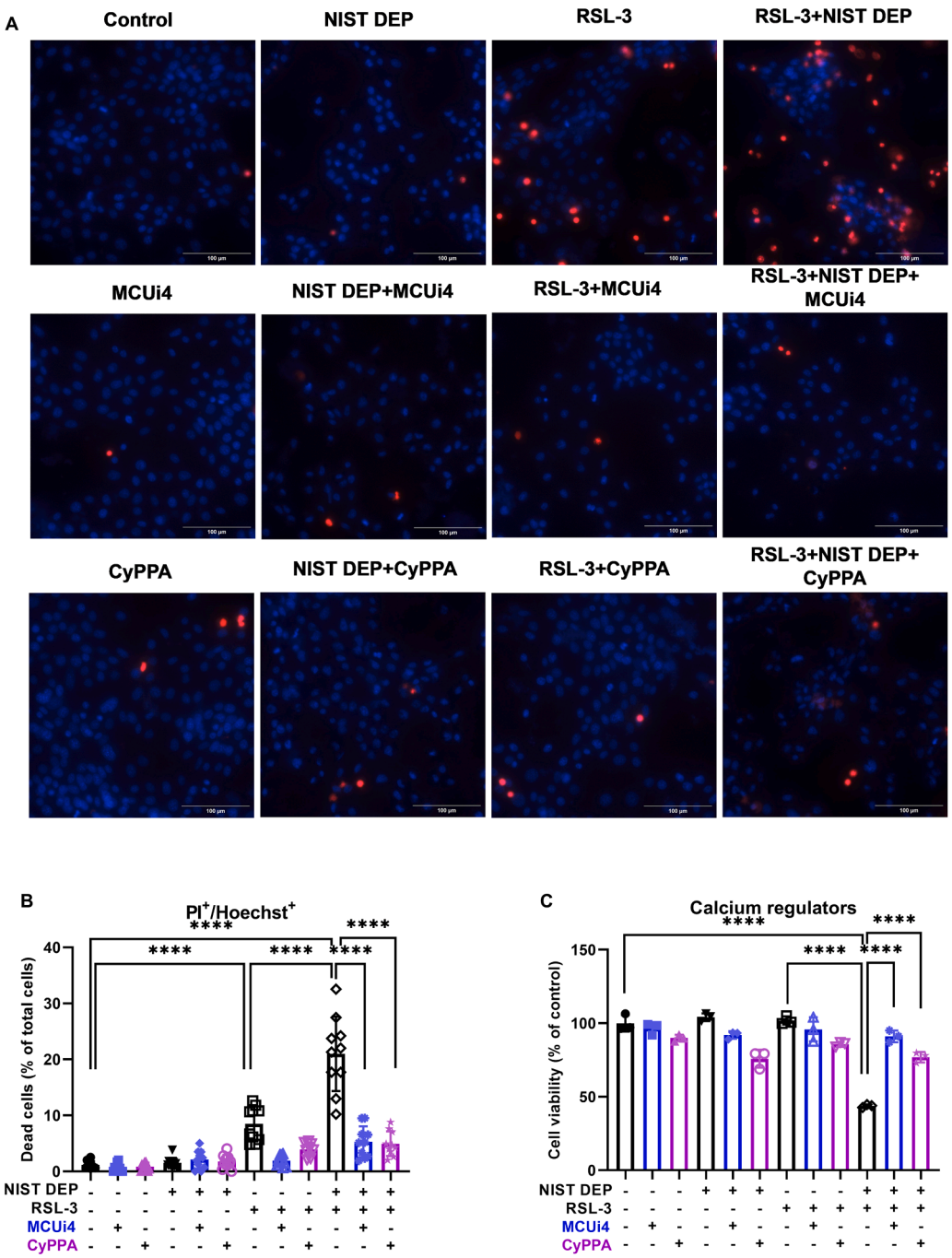

Fig. 5. HT22 ferroptotic cell death induced by RSL-3 and NIST DEP is alleviated by inhibition of mitochondrial calcium uptake. (A) PI/Hoechst 33342 double-stained fluorescence images at 40x magnification after 17 hrs exposure to NIST DEP, RSL-3, calcium regulators MCUi4 (5 μM) and CyPPA (10 μM) alone or in combination. Red: dead cells, Blue: nucleus (scale bar =100 μm). (B) Quantitative analysis of PI-positive cells was performed based on 10 fluorescent images per condition (mean ± SD). The percentage of dead cells in the control group was defined as 100 %. (C) MTT assay for the viability of HT22 cells after 17 hrs exposure to NIST DEP, RSL-3, calcium regulators MCUi4 (5 μM) and CyPPA (10 μM) alone or in combination. The cell viability of the control group was defined as 100 %. Statistical analysis was performed using one-way ANOVA followed by Tukey's post hoc multiple comparison test. $^{****}p < 0.0001$. All experiments were repeated at least three times as biological replicates.

morphology is altered upon exposure to NIST DEP, by using fluorescence microscopy. Mitotracker Red staining revealed that mitochondrial morphology was elongated and tubular in both control and cells exposed to NIST DEP. In contrast, exposure to RSL-3 induced mitochondrial fragmentation (Fig. 6A), while the subsequent addition of NIST DEP exacerbated this damage, leading to the formation of more aggregated and fragmented mitochondria. Interestingly, co-treatment with MCUi4 and CyPPA significantly prevented the mitochondrial fragmentation, and restored normal mitochondrial morphology (Fig. 6B).

The analysis using ImageJ plugin for mitochondrial morphology showed that the skeleton images of the mitochondrial structures were different upon various treatments [56]. In agreement with the lack of profound alterations in HT22 cells upon exposure to NIST DEP alone (Figs. 5B, 5C) in terms of cell viability, there was almost no effect on the four mitochondrial network parameters compared to the control group (Figs. 6C, 6D, S4A, S4B). Mitochondrial network structure represented by mitochondrial footprints was slightly reduced in the RSL-3 alone--treated cells (195.4 ± 29.2 μm^2) compared with control cells (221.5

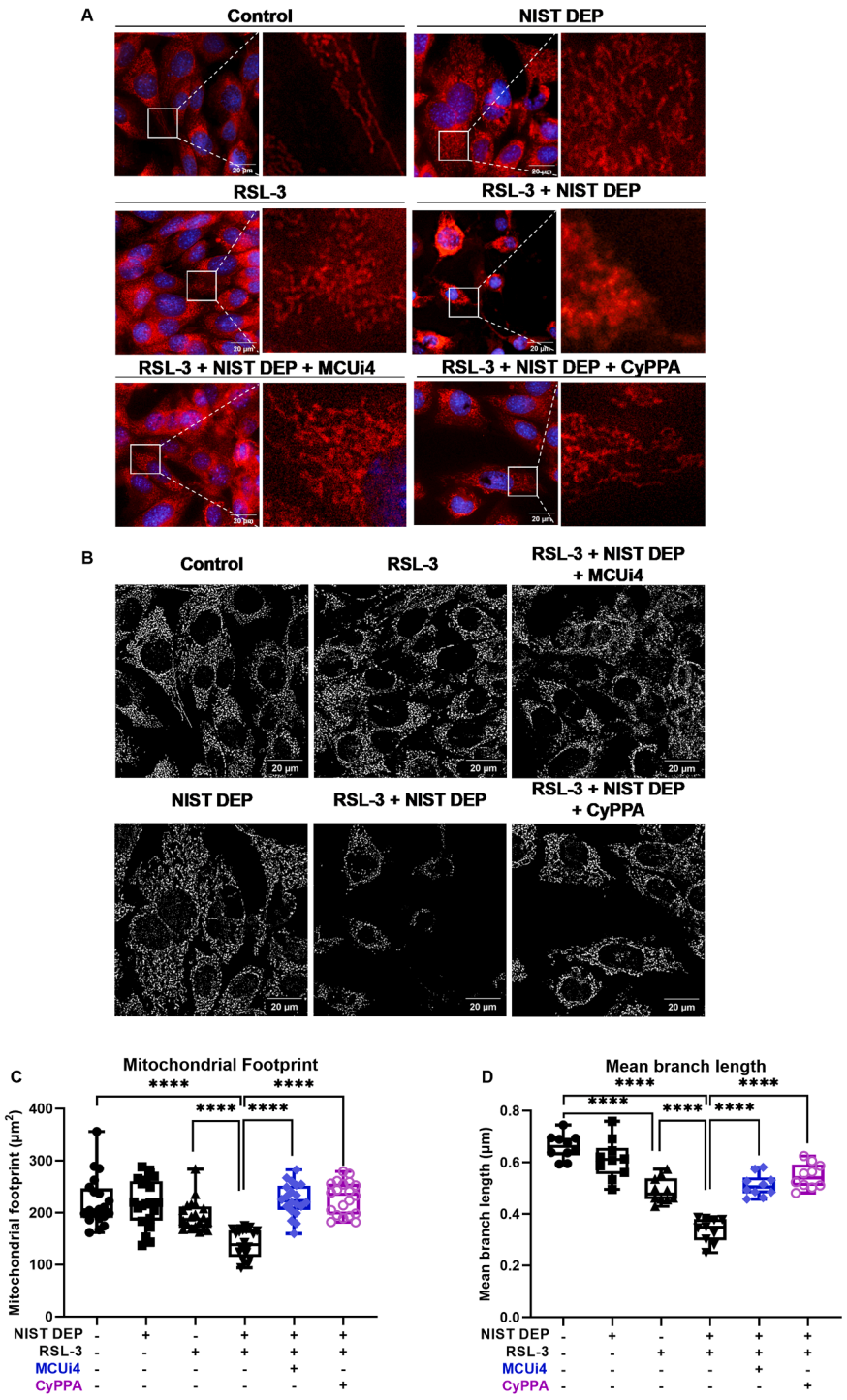

Fig. 6. Co-exposure to RSL-3 and NIST DEP induce mitochondrial morphological alteration. (A) Mitotracker Red fluorescence images at 63x magnification after 17 hrs exposure to NIST DEP and RSL-3 alone and in combination with or without the calcium regulators MCUi4 (5 μM) and CyPPA (10 μM). Red: mitochondrial, Blue: nucleus (scale bar = 20 μm). Enlarged images of the boxed area are shown in the right panels. (B) Mitochondrial skeleton images at 63x magnification after 17 hrs exposure to NIST DEP and RSL-3 alone and in combination with or without the calcium regulators MCUi4 (5 μM) and CyPPA (10 μM). (C-D) Parameters of HT22 mitochondrial network morphology analysis after different treatments: (C) Mitochondrial footprint. 15 single cells were analyzed for each condition. (D) Mean branch length. 10 whole fluorescence images were analyzed for each condition. Statistical analysis was performed using one-way ANOVA followed by Tukey's post hoc multiple comparison test. $^{****}p < 0.0001$. All experiments were repeated at least three times as biological replicates.

$\pm$ 48.0 μm^2) (Fig. 6C), and the reduction was more dramatic upon co-exposure to NIST DEP (140.2 $\pm$ 27.2 μm^2). These findings were consistent with the extent of mitochondrial damage shown in Fig. 6A. Importantly, the addition of MCUi4 (225.2 $\pm$ 31.2 μm^2) or CyPPA (228.8 $\pm$ 31.7 μm^2) prevented mitochondrial footprints and other parameters of mitochondrial integrity compared with RSL-3 and NIST DEP co-treatment cells (Figs. 6C, 6D, S4A, S4B). These results suggested that NIST DEP exposure would further interfere with the mitochondrial fragmentation of ferroptotic-sensitized cells.

3.7. Combined exposure to NIST DEP and RSL-3 mediates lipid peroxidation and increases in mitochondrial ROS

The accumulation of lipid peroxidation in cells is one of the important characteristics of ferroptosis [57]. Therefore, the effect of lipid peroxidation in the presence of combined NIST DEP and RSL-3 exposure was studied by analyzing the shift in fluorescence color from red to green of the fluorescent dye BODIPY 581/591 C11 [58] (Fig. 7A). We next quantified the intensity of the red and green fluorescence signals, and the ratio results were shown in Fig. 7B. NIST DEP exposure slightly increased the ratio of green fluorescence to red fluorescence compared to the control group from 102.7 ± 30.3 % to 117.8 ± 28.6 %. However, the combined exposure to RSL-3 and NIST DEP (218.0 ± 43.8 %) showed a further increase in the ratio compared to the RSL-3 alone group (137.2 ± 44.0 %) (Figs. 7A, 7B). The addition of MCUi4 or CyPPA significantly weakened the signal of the oxidized green probe compared to the RSL-3 and NIST DEP co-treatment cells from 218.0 ± 43.8 % to 113.7 ± 39.2 % (MCUi4) and to 103.2 ± 18.6 % (CyPPA).

These results indicated that MCUi4 and CyPPA could reduce the level of lipid peroxidation mediated by the NIST DEP and RSL-3 challenge

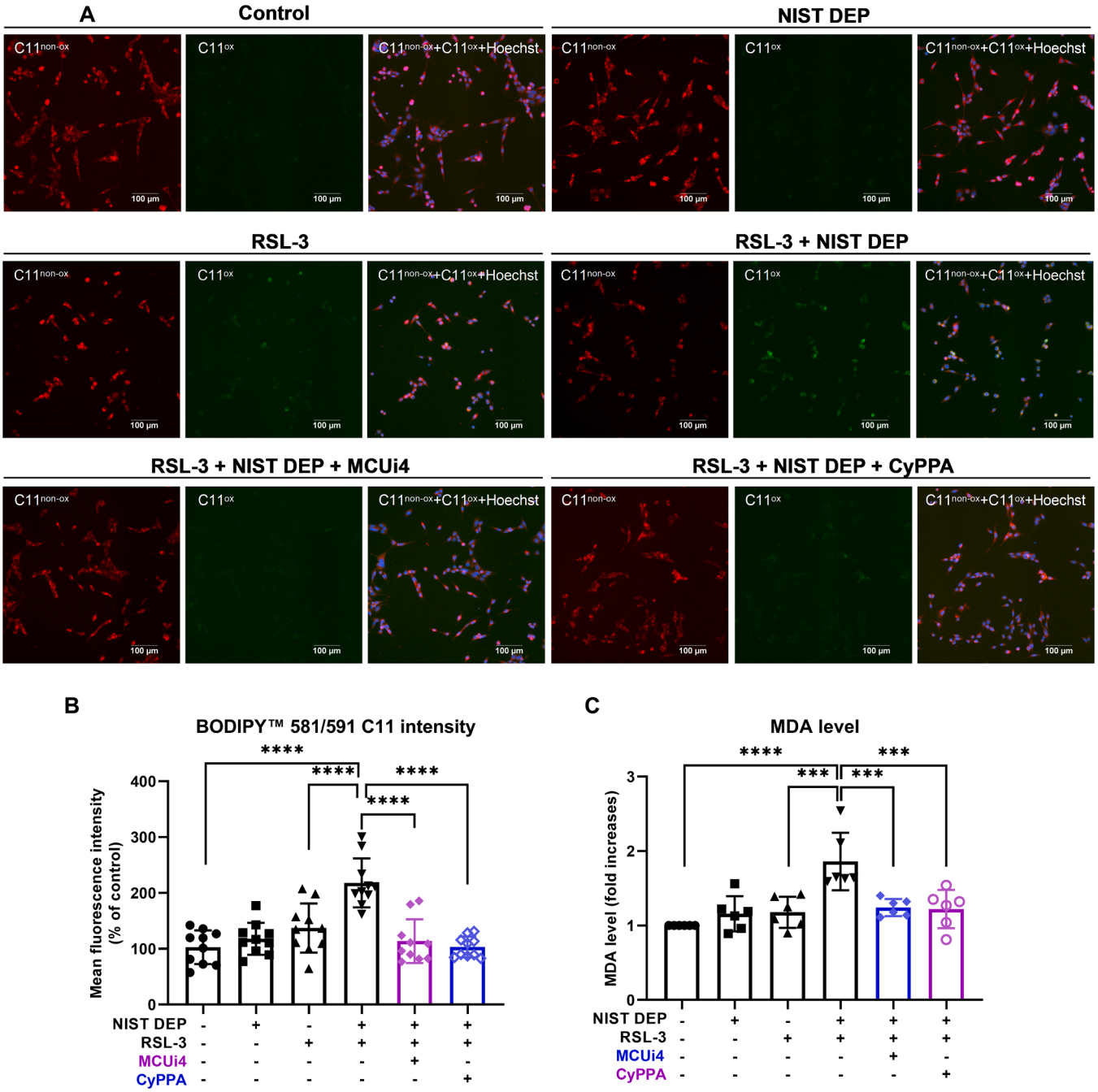

Fig. 7. Lipid peroxidation induced by RSL-3 and NIST DEP can be alleviated by MCUi4 and CyPPA. (A) BODIPY 581/591 C11fluorescence images at 20x magnification after 6 hrs exposure to NIST DEP and RSL-3 alone and in combination with or without the calcium regulators MCUi4 (5 μM) and CyPPA (10 μM). Red: C11non-ox, Green: C11ox, Blue: nucleus (scale bar = 100 μm). (B) Quantitative analysis of BODIPY 581/591 C11 mean fluorescence intensity was performed based on 10 fluorescent images per condition (mean ± SD). (C) MDA levels after 6 hrs of different treatments. All conditions were normalized by their corresponding protein concentrations, and the MDA concentration of the control group was defined as 1. Statistical analysis was performed using one-way ANOVA followed by Tukey's post hoc multiple comparison test. $^{***}p < 0.001$, $^{****}p < 0.0001$. All experiments were repeated at least three times as biological replicates.

(Figs. 7A, 7B). To further substantiate the measurement of lipid peroxidation, the aldehyde compound MDA produced by the decomposition of polyunsaturated fatty acids after exposure to oxidative stress was measured [59]. NIST DEP exposure and RSL-3 treatment alone resulted in both a 1.2 ± 0.2 - fold increase in MDA production compared with controls. Meanwhile, the amount of MDA increased to 1.9 ± 0.4 - fold with the addition of NIST DEP and RSL-3 compared to the solvent-treated cells. In contrast, both MCUi4 (1.2 ± 0.1 - fold) and CyPPA (1.2 ± 0.3 - fold) almost completely eliminated the increase in MDA levels caused by NIST DEP and RSL-3 (1.9 ± 0.4 - fold) (Fig. 7C). Mitochondrial ROS levels are used as indicators of metabolic stress and cell damage [54]. Following various treatments, the generation of ROS in mitochondria of HT22 cells was measured using the red fluorescence probe, MitoSOX. The red fluorescence intensity was enhanced to 1.2 ± 0.1 - fold upon RSL-3 treatment, and further enhanced to 1.4 ± 0.5 - fold in the RSL-3 and NIST DEP co-treated cells. Importantly, the addition of MCUi4 or CyPPA both significantly attenuated the red signal to 1.1 ± 0.1 - fold (Fig. S5A, S5B). Subsequently, quantitative analysis based on image fluorescence intensity showed consistent results indicating that inhibition of mitochondrial calcium can prevent cellular changes that occur upon exposure to NIST DEP particles in RSL-3 sensitized cells (Fig. S5B, S5C).

4. Discussion

Our data showed for the first time that air pollutants, exampled here with NIST DEP, are able to potentiate ferroptotic sensitivity to neuronal cell death. As this cell death type involves an exogenous, or foreign signal to ignite the cell death in conditions of small increases of lipid peroxidation, we term this cell death type xenoferroptosis. The xenoferroptotic cell death is distinct from ferroptosis as an external stimulus unrelated to lipid peroxidation could accelerate cell death in cells vulnerable to ferroptosis (Fig. 8).

Our study also demonstrated the involvement of mitochondrial calcium uniporter and mitochondrial calcium in the xenoferroptotic cell death pathway. Moreover, our findings indicated that targeting mitochondrial calcium and SK channels could represent potential therapeutic targets to prevent this xenoferroptotic cell death.

An increasing number of research suggested that air pollutants strongly correlated with neurodegenerative diseases and even reached the central nervous system by penetrating the blood brain barrier via various routes [60]. Particulate matter (PM) exposure impaired the spatial learning and memory abilities of postnatal 28-day Sprague Dawley juvenile rats, processes accompanied by a change in the morphology and structure of their hippocampus [61]. In addition, previous research has shown that organic extracts in PM2.5 could induce ferroptosis in SH-SY5Y cells. It is worth noting that the metabolic activity of HT22 cells was not significantly affected by NIST DEP up to a concentration of 100 μg/mL. Other studies have shown that exposure to NIST DEP for 3 h or 24 h did not cause significant cell death in HT22 cells [62]. In addition, there was no significant decrease in cell viability of human bronchial epithelial cells BEAS-2B after treatment with NIST DEP at concentrations up to 20 μg/cm^2 for 24 h [63], but NIST DEP only changed cell viability at concentrations higher than 300 μg/mL and periods of time longer than 72 h [64]. We next investigated the role of NIST DEP in ferroptosis-sensitive cells. RSL-3 can induce ferroptosis by inhibiting the activity of glutathione peroxidase 4 (GPX4) [65]. Therefore, RSL-3 was used as a ferroptosis inducer in our study. HT22 cells are a mouse-derived immortalized neuronal cell line that are sensitive to oxidative stress and susceptible to ferroptosis triggered by the loss of GPX4. Therefore, HT22 cells represent an ideal model for studying the mechanisms of ferroptosis [36,42,66]. Importantly, combined treatment with NIST DEP and RSL-3 of HT22 cells, further reduced the cell viability compared to treatment with RSL-3 alone. Subsequently, the ferroptosis inhibitor Fer-1 and the apoptosis inhibitor QVD were used to verify the cell death mode mediated by the addition of NIST DEP. The addition of Fer-1 but not of QVD abolished the impact of NIST DEP plus RSL-3 on HT22 cell viability indicating that ferroptosis is the main form of cell death is operational in cells challenged with both NIST DEP and RSL-3. In line with our findings, other findings showed that PM2.5 can cause ferroptosis in epithelial cells, as the addition of ferroptosis inhibitor Fer-1 and iron chelator DFOM could alleviate the decrease in cell

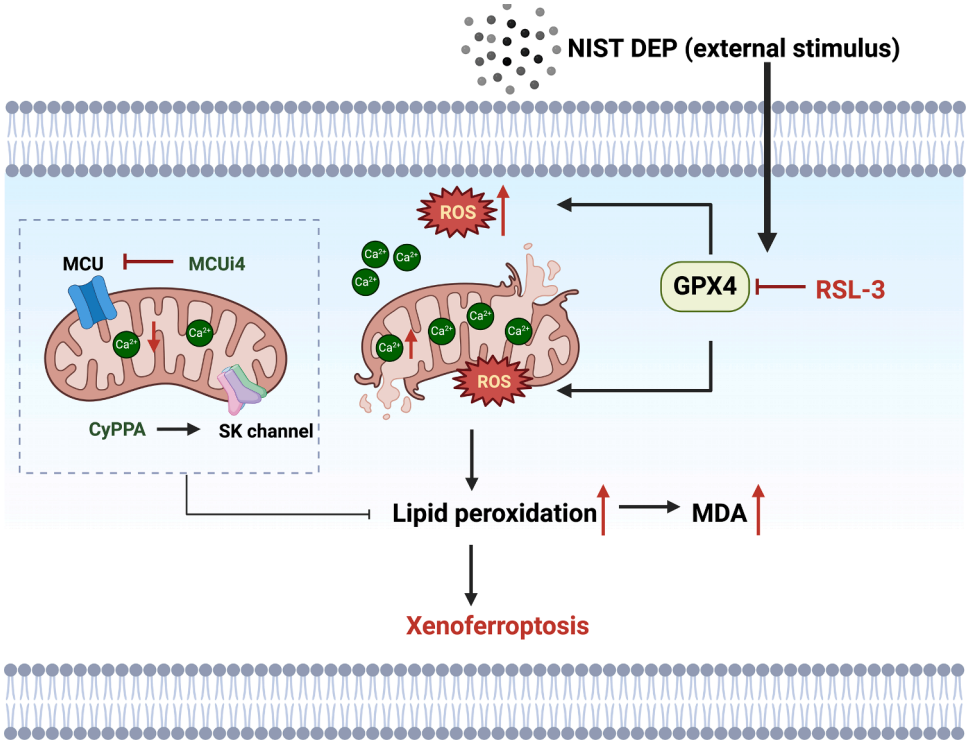

Fig. 8. The xenoferroptotic pathway involves lipid peroxidation and an external stimulus accelerating the cell death. This figure was created with BioRender.

viability caused by PM2.5 [67].

Excessive increase of intracellular calcium was associated with the ferroptosis-cell death pathway [20]. Modulation of mitochondrial calcium by inhibiting the MCU complex by MCUi4 or activating SK channels by CyPPA have been linked to ferroptosis pathways in HT22 cells and primary cortical neurons. [37,42]. Therefore, the MCU complex inhibitor MCUi4 and the SK channel activator CyPPA were used to test how the modulation of calcium could interfere with the effects mediated by exposure to NIST DEP in RSL-3-sensitised cells. Cell exposure to combined NIST DEP and RSL-3 showed increased intracellular and mitochondrial calcium levels. In line with our findings, PM2.5 significantly increased the intracellular calcium levels of rat alveolar macrophages and HaCaT cells in a concentration-dependent manner [68,69]. PM2.5 can damage the mitochondrial structure and the ability of a murine cardiomyocyte cell HL-1 to regulate calcium fluctuations required for heart rate regulation [70]. In our study, both MCUi4 and CyPPA could attenuate the intracellular calcium levels induced by NIST DEP and RSL-3 addition. In addition, asbestos particles increased mitochondrial calcium uptake by promoting overexpression of MCU in mouse MH-S alveolar macrophages [71]. Therefore, our results further demonstrated that MCUi4 effectively alleviated NIST DEP-induced calcium imbalance by blocking the MCU pathway.

The ER-mitochondria calcium pathway is an important pathway for regulating intracellular calcium homeostasis [72]. Increased contact sites between ER and mitochondria occur in many neurodegenerative diseases [73]. In our study, we observed that exposure to NIST DEP and RSL-3 significantly increased the number of ER-mitochondrial contact sites, while MCUi4 and CyPPA restored contact sites to control levels. Subsequently, mitochondrial calcium levels were elevated in response to NIST DEP and RSL-3 exposure, while MCUi4 and CyPPA reduced this increase to the level of the control group.

Consistent with our findings, PM2.5 exposure significantly increased mitochondrial calcium levels in bronchial epithelial BEAS-2B cells and skin cells HaCaT and NHDF [74,75]. Our results suggested the challenge posed by NIST DEP to HT22 cells may be caused by a disruption of calcium homeostasis.

Mitochondrial calcium plays a crucial role in the regulation of mitochondrial morphology by regulating its metabolism and dynamic processes. Exposure to NIST DEP in RSL-3-sensitised cells caused changes in the mitochondrial morphology of HT22, showing more severe fragmentation compared to the either RSL-3/NIST DEP treatment alone or solvent-treated control cells. The use of MCUi4 and CyPPA restored mitochondrial morphology, comparable to healthy cells. Liu et al. (2024) reported reduced mitochondrial fragmentation and grid connections in lung epithelial cells BEAS-2B after PM2.5 exposure and Fang et al. (2022) observed that exposure to cigarette smoke extract significantly disrupted the morphology and increased the fragmentation of mitochondria in primary human airway smooth cells [56,76]. These results showed NIST DEP could intensify RSL-3-induced ferroptosis by exacerbating mitochondrial fragmentation.

Lipid peroxidation and accumulation of ROS are key features of ferroptotic cell death [77,78]. In our study, NIST DEP further increased lipid peroxidation and mitochondrial ROS levels initiated by RSL-3 treatment, while the addition of MCUi4 and CyPPA reduced the increase in oxidative stress. In addition, measurements of the MDA content paralleled the lipid peroxidation levels. Studies have reported that PM2.5 exposure can increase the levels of MDA and lipid ROS in SH-SY5Y cells in a concentration-dependent manner [79]. Moreover, PM could induce the production of mitochondrial ROS in a human colon adenocarcinoma Caco-2 cells [80]. Until now, no studies reported the protective effect of the inhibition of the mitochondrial calcium uniporter complex or activation of SK channels in relation to the air pollutants cellular effects. Therefore, this study provideed key insights into the potential harm mediated by air pollutants, particularly NIST DEP in conditions in which cells were sensitized to lipid peroxidation and cellular ROS. NIST DEP alone had minimal effects on cellular processes, while in cells sensitized to ferroptotic pathway, the cell death was amplified and accelerated. Calcium signaling and mitochondrial ROS are essential elements in this cell type death in which a foreign stimulus is facilitating ferroptotic cell death in cells with increased lipid peroxidation. Our study revealed that catalyzing ferroptotic cell death is dependent on increases in mitochondrial calcium and inhibitions of mitochondrial calcium uniporter complex or activation of SK channels could represent novel therapeutic targets against the xenoferroptotic cell death.

We acknowledge certain limitations in our current study, while still recognizing the importance of *in vitro* neuronal cell system for better understanding molecular pathways relevant to NIST-DEP exposure. Although, the HT22 cells may not fully reflect the biological characteristics of native brain neurons, they represent a good model to study ferroptosis, as they lack NMDA receptors therefore glutamate is not capable to induce excitotoxicity or apoptosis. These cells express xCT transporter that once inhibited by glutamate will result in decrease GSH and increased lipid peroxidation. Therefore, this cell model is allowing a better investigation of distinct ferroptotic processes without involvement of apoptotic or other cell death pathways. However, future research could incorporate neuronal models derived from human induced pluripotent stem cells to enhance physiological relevance and broaden applicability [81]. Additionally, although *in vitro* systems provide crucial mechanistic insights, they do not completely replicate the complex *in vivo* environment, including the blood-brain barrier, immune system [82], and tissue microenvironment. Therefore, further exploration using animal models or organoid systems could support to deepen our understanding of the neurotoxicity of NIST DEP and its potential influence on neurodegenerative diseases [83].

5. Conclusions

In summary, the current study investigated the potential harm of NIST DEP to ferroptosis-sensitive cells and further studied the mechanisms related to calcium pathways. The results demonstrated that NIST DEP-induced acceleration of xenoferroptosis mainly through calcium dysregulation, lipid peroxidation and ROS accumulation. Therefore, modulation of calcium homeostasis is one of the therapeutic strategies for the negative effects of particulate matter (especially NIST DEP) on the brain.

Environmental implication

Diesel exhaust particles (DEP) are major component of traffic-related PM, posing a threat to the environment and human health. With increasing evidence of PM in brain tissue, environmental factors are considered to contribute significantly to the development of neurodegenerative diseases. However, the mechanisms underlying NIST DEP-accelerated ferroptosis still require further investigation. Our data show for the first time that air pollutants, exemplified by NIST DEP, can enhance the sensitivity of neuronal cell death to ferroptosis and explain the potential mechanisms of this adverse effect. Our study is of great significance for environmental protection and treatment of neurodegenerative diseases.

Abbreviations

NIST: National Institute of Sciences and Technology
DEP: diesel exhaust particles
AD: Alzheimer's disease
PD: Parkinson's disease
ALS: amyotrophic lateral sclerosis
GBD: Global Burden of Disease
WHO: World Health Organization
CNS: central nervous system
ROS: reactive oxygen species

Ca^{2+}: calcium
SK: small conductance calcium-activated potassium
MCU: mitochondrial calcium uniporter
MDA: malondialdehyde
MitoROS: mitochondrial ROS
MTT: 3-(4,5-Dimethyl-2-thiazolyl)-2,5-diphenyl-2H-tetrazolium bromide
DMSO: dimethyl sulfoxide
PI: propidium iodide
TBARS: Thiobarbituric acid reactive substances
ER: Endoplasmic reticulum
PM: particulate matter
GPX4: glutathione peroxidase 4

CRediT authorship contribution statement

Leshan Zhang: Writing – review & editing, Writing – original draft, Visualization, Methodology, Investigation, Formal analysis, Conceptualization. **Hong Yan:** Writing – review & editing, Writing – original draft, Visualization, Methodology, Investigation, Conceptualization. **Mohammad Saidur Rahman:** Visualization, Validation, Methodology, Investigation. **Christina Mol-van der Veen:** Visualization, Validation, Methodology, Investigation, Formal analysis. **Ana Manzano Covarrubias:** Visualization, Methodology, Investigation. **Karim Rafie:** Supervision, Methodology, Investigation. **Diana Pendin:** Writing – original draft, Validation, Resources, Methodology. **Martina Schmidt:** Writing – review & editing, Writing – original draft, Supervision, Project administration, Investigation, Conceptualization. **Amalia Dolga:** Writing – review & editing, Writing – original draft, Supervision, Project administration, Investigation, Funding acquisition, Conceptualization.

Declaration of Competing Interest

The authors declare that they have no known competing financial interests or personal relationships that could have appeared to influence the work reported in this paper.

Acknowledgments

Leshan Zhang is a recipient of the China Scholarship Council (CSC, 202206300004). Hong Yan is a recipient of the China Scholarship Council (CSC, 202006300052). Amalia M Dolga is the recipient of an Alzheimer Nederland grant (WE.03–2018–04, the Netherlands), Parkinson Fonds (the Netherlands), and a Rosalind Franklin Fellowship co-funded by the European Union and the University of Groningen. Martina Schmidt received support by Alzheimer Nederland grant (WE.03–2019–05) and Deutsche Forschungsgemeinschaft (IRTG1874-DIAMICOM-SP2) and Novartis unrestricted grant (50199468).

Appendix A. Supporting information

Supplementary data associated with this article can be found in the online version at doi:10.1016/j.jhazmat.2025.137374.

Data availability

Data will be made available on request.

References

[1] Cieri, D., Brini, M., Calì, T., 2017. Emerging (and converging) pathways in Parkinson's disease: keeping mitochondrial wellness. Biochem Biophys Res Commun 483, 1020–1030.
[2] Giorgi, C., Danese, A., Missiroli, S., Patergnani, S., Pinton, P., 2018. Calcium dynamics as a machine for decoding signals. Trends Cell Biol 28, 258–273.
[3] Walters, G.C., Usachev, Y.M., 2023. Mitochondrial calcium cycling in neuronal function and neurodegeneration. Front Cell Dev Biol 11, 1094356.
[4] Krabbendam, I.E., Honrath, B., Culmsee, C., Dolga, A.M., 2018. Mitochondrial Ca2 + -activated K+ channels and their role in cell life and death pathways. Cell Calcium 69, 101–111.
[5] Krabbendam, I.E., Honrath, B., Dilberger, B., Iannetti, E.F., Branicky, R.S., Meyer, T., Evers, B., Dekker, F.J., Koopman, W.J., Beyrath, J., 2020. SK channel-mediated metabolic escape to glycolysis inhibits ferroptosis and supports stress resistance in C. elegans. Cell death Dis 11, 263.
[6] Dudem, S., Sergeant, G.P., Thornbury, K.D., Hollywood, M.A., 2021. Calcium-activated K+ channels (KCa) and therapeutic implications. In: Pharmacology of Potassium Channels. Springer, pp. 379–416.
[7] Choudhury, S.P., Bano, S., Sen, S., Suchal, K., Kumar, S., Nikolajeff, F., Dey, S.K., Sharma, V., 2022. Altered neural cell junctions and ion-channels leading to disrupted neuron communication in Parkinson's disease. npj Park'S Dis 8, 66.
[8] Honrath, B., Krabbendam, I.E., Culmsee, C., Dolga, A.M., 2017. Small conductance Ca2+ -activated K+ channels in the plasma membrane, mitochondria and the ER: pharmacology and implications in neuronal diseases. Neurochem Int 109, 13–23.
[9] Matschke, L.A., Rinné, S., Snutch, T.P., Oertel, W.H., Dolga, A.M., Decher, N., 2018. Calcium-activated SK potassium channels are key modulators of the pacemaker frequency in locus coeruleus neurons. Mol Cell Neurosci 88, 330–341.
[10] Trombetta-Lima, M., Krabbendam, I.E., Dolga, A.M., 2020. Calcium-activated potassium channels: Implications for aging and age-related neurodegeneration. Int J Biochem Cell Biol 123, 105748.
[11] Honrath, B., Krabbendam, I.E., IJsebaart, C., Pegoretti, V., Bendridi, N., Rieusset, J., Schmidt, M., Culmsee, C., Dolga, A.M., 2018. SK channel activation is neuroprotective in conditions of enhanced ER–mitochondrial coupling. Cell death Dis 9, 593.
[12] Baev, A.Y., Vinokurov, A.Y., Novikova, I.N., Dremin, V.V., Potapova, E.V., Abramov, A.Y., 2022. Interaction of mitochondrial calcium and ROS in neurodegeneration. Cells 11, 706.
[13] Alevriadou, B.R., Patel, A., Noble, M., Ghosh, S., Gohil, V.M., Stathopulos, P.B., Madesh, M., 2021. Molecular nature and physiological role of the mitochondrial calcium uniporter channel. Am J Physiol-Cell Physiol.
[14] Groten, C.J., MacVicar, B.A., 2022. Mitochondrial Ca2+ uptake by the MCU facilitates pyramidal neuron excitability and metabolism during action potential firing. Commun Biol 5, 900.
[15] Boyman, L., Karbowski, M., Lederer, W.J., 2020. Regulation of mitochondrial ATP production: Ca2+ signaling and quality control. Trends Mol Med 26, 21–39.
[16] Sun, Y., Yan, C., He, L., Xiang, S., Wang, P., Li, Z., Chen, Y., Zhao, J., Yuan, Y., Wang, W., 2023. Inhibition of ferroptosis through regulating neuronal calcium homeostasis: an emerging therapeutic target for Alzheimer's disease. Ageing Res Rev 87, 101899.
[17] Lewerenz, J., Ates, G., Methner, A., Conrad, M., Maher, P., 2018. Oxytosis/ferroptosis—(Re-) emerging roles for oxidative stress-dependent non-apoptotic cell death in diseases of the central nervous system. Front Neurosci 12, 214.
[18] Majerníková, Na, den Dunnen, W.F., Dolga, A.M., 2021. The potential of ferroptosis-targeting therapies for Alzheimer's disease: from mechanism to transcriptomic analysis, Frontiers in Aging. Neuroscience 13, 745046.
[19] Marmolejo-Garza, A., Dolga, A.M., 2021. PEG out through the pores with the help of ESCRTIII. Cell Calcium 97, 102422.
[20] Gleitze, S., Paula-Lima, A., Núñez, M.T., Hidalgo, C., 2021. The calcium–iron connection in ferroptosis-mediated neuronal death. Free Radic Biol Med 175, 28–41.
[21] Xu, Y., Zhao, J., Zhao, Y., Zhou, L., Qiao, H., Xu, Q., Liu, Y., 2023. The role of ferroptosis in neurodegenerative diseases. Mol Biol Rep 50, 1655–1661.
[22] Lamptey, R.N., Chaulagain, B., Trivedi, R., Gothwal, A., Layek, B., Singh, J., 2022. A review of the common neurodegenerative disorders: current therapeutic approaches and the potential role of nanotherapeutics. Int J Mol Sci 23, 1851.
[23] Liu, X.-q, Huang, J., Song, C., Zhang, T.-l, Liu, Y.-p, Yu, L., 2023. Neurodevelopmental toxicity induced by PM2. 5 exposure and its possible role in neurodegenerative and mental disorders. Hum Exp Toxicol 42, 09603271231191436.
[24] Chen, J.C., Wang, X., Wellenius, G.A., Serre, M.L., Driscoll, I., Casanova, R., McArdle, J.J., Manson, J.E., Chui, H.C., Espeland, M.A., 2015. Ambient air pollution and neurotoxicity on brain structure: evidence from women's health initiative memory study. Ann Neurol 78, 466–476.
[25] Power, M.C., Weisskopf, M.G., Alexeeff, S.E., Coull, B.A., Spiro III, A., Schwartz, J., 2011. Traffic-related air pollution and cognitive function in a cohort of older men. Environ Health Perspect 119, 682–687.
[26] Ranft, U., Schikowski, T., Sugiri, D., Krutmann, J., Krämer, U., 2009. Long-term exposure to traffic-related particulate matter impairs cognitive function in the elderly. Environ Res 109, 1004–1011.
[27] Weuve, J., Puett, R.C., Schwartz, J., Yanosky, J.D., Laden, F., Grodstein, F., 2012. Exposure to particulate air pollution and cognitive decline in older women. Arch Intern Med 172, 219–227.
[28] Calderón-Garcidueñas, L., Mora-Tiscareño, A., Ontiveros, E., Gómez-Garza, G., Barragán-Mejía, G., Broadway, J., Chapman, S., Valencia-Salazar, G., Jewells, V., Maronpot, R.R., 2008. Air pollution, cognitive deficits and brain abnormalities: a pilot study with children and dogs. Brain Cogn 68, 117–127.
[29] Maher, B.A., Ahmed, I.A., Karloukovski, V., MacLaren, D.A., Foulds, P.G., Allsop, D., Mann, D.M., Torres-Jardón, R., Calderon-Garciduenas, L., 2016. Magnetite pollution nanoparticles in the human brain. Proc Natl Acad Sci 113, 10797–10801.
[30] Manzano-Covarrubias, A.L., Yan, H., Luu, M.D.A., Gadjdjoe, P.S., Dolga, A.M., Schmidt, M., 2023. Unravelling the signaling power of pollutants. Trends Pharmacol Sci 44, 917–933.

[31] World Health Organization, 2023.. Air Pollut. https://www.who.int/health-topics/air-pollution#tab=tab_1.
[32] Manisalidis, I., Stavropoulou, E., Stavropoulos, A., Bezirtzoglou, E., 2020. Environmental and health impacts of air pollution: a review. Front Public Health 8, 14.
[33] Yang, L., Cai, X., Li, R., 2024. Ferroptosis induced by pollutants: an emerging mechanism in environmental toxicology. Environ Sci Technol 58, 2166–2184.
[34] Wu, T., Wang, X., Cheng, J., Liang, X., Li, Y., Chen, M., Kong, L., Tang, M., 2022. Nitrogen-doped graphene quantum dots induce ferroptosis through disrupting calcium homeostasis in microglia. Part Fibre Toxicol 19, 22.
[35] Park, S.Y., An, K.S., Lee, B., Kang, J.H., Jung, H.J., Kim, M.W., Ryu, H.Y., Shim, K. S., Nam, K.T., Yoon, Y.S., Oh, S.H., 2021. Establishment of particulate matter-induced lung injury model in mouse. Lab Anim Res 37, 12.
[36] Kritis, A.A., Stamoula, E.G., Paniskaki, K.A., Vavilis, T.D., 2015. Researching glutamate–induced cytotoxicity in different cell lines: a comparative/collective analysis/study. Front Cell Neurosci 9, 91.
[37] Zhang, Y., Shaabani, S., Vowinkel, K., Trombetta-Lima, M., Sabogal-Guáqueta, A. M., Chen, T., Hoekstra, J., Lembeck, J., Schmidt, M., Decher, N., 2024. Novel SK channel positive modulators prevent ferroptosis and excitotoxicity in neuronal cells. Biomed Pharmacother 171, 116163.
[38] Li, N., Hao, M., Phalen, R.F., Hinds, W.C., Nel, A.E., 2003. Particulate air pollutants and asthma: a paradigm for the role of oxidative stress in PM-induced adverse health effects. Clin Immunol 109, 250–265.
[39] Wei, M., Bao, G., Li, S., Yang, Z., Cheng, C., Le, W., 2022. PM2. 5 exposure triggers cell death through lysosomal membrane permeabilization and leads to ferroptosis insensitivity via the autophagy dysfunction/p62-KEAP1-NRF2 activation in neuronal cells. Ecotoxicol Environ Saf 248, 114333.
[40] Wang, Y., Zhang, M., Li, Z., Yue, J., Xu, M., Zhang, Y., Yung, K.K.L., Li, R., 2019. Fine particulate matter induces mitochondrial dysfunction and oxidative stress in human SH-SY5Y cells. Chemosphere 218, 577–588.
[41] Xiong, Q., Tian, X., Xu, C., Ma, B., Liu, W., Sun, B., Ru, Q., Shu, X., 2022. PM2. 5 exposure-induced ferroptosis in neuronal cells via inhibiting ERK/CREB pathway. Environ Toxicol 37, 2201–2213.
[42] Marmolejo-Garza, A., Krabbendam, I.E., Luu, M.D.A., Brouwer, F., Trombetta-Lima, M., Unal, O., O'Connor, S.J., Majerníková, N., Elzinga, C.R., Mammucari, C., 2023. Negative modulation of mitochondrial calcium uniporter complex protects neurons against ferroptosis. Cell Death Dis 14, 772.
[43] Nie, C., Zhou, J., Qin, X., Shi, X., Zeng, Q., Liu, J., Yan, S., Zhang, L., 2016. Reduction of apoptosis by proanthocyanidin-induced autophagy in the human gastric cancer cell line MGC-803. Oncol Rep 35, 649–658.
[44] De Nadai, A., Vajente, N., Pendin, D., Mattarei, A., 2021. Mt-fura-2, a ratiometric mitochondria-targeted Ca2+ sensor. Determination of spectroscopic properties and Ca2+ imaging assays. In: Mitochondrial Medicine: Volume 1: Targeting Mitochondria. Springer, pp. 187–215.
[45] Pendin, D., Norante, R., De Nadai, A., Gherardi, G., Vajente, N., Basso, E., Kaludercic, N., Mammucari, C., Paradisi, C., Pozzan, T., 2019. A synthetic fluorescent mitochondria-targeted sensor for ratiometric imaging of calcium in live cells. Angew Chem Int Ed 58, 9917–9922.
[46] Trollinger, D.R., Cascio, W.E., Lemasters, J.J., 1997. Selective loading of Rhod 2 into mitochondria shows mitochondrial Ca2+ transients during the contractile cycle in adult rabbit cardiac myocytes. Biochem Biophys Res Commun 236, 738–742.
[47] Valente, A.J., Maddalena, L.A., Robb, E.L., Moradi, F., Stuart, J.A., 2017. A simple ImageJ macro tool for analyzing mitochondrial network morphology in mammalian cell culture. Acta Histochem 119, 315–326.
[48] Chaudhry, A., Shi, R., Luciani, D.S., 2020. A pipeline for multidimensional confocal analysis of mitochondrial morphology, function, and dynamics in pancreatic β-cells. Am J Physiol-Endocrinol Metab 318, E87–E101.
[49] Murray, M.B., Leak, L.B., Lee, W.C., Dixon, S.J., 2023. Protocol for detection of ferroptosis in cultured cells. STAR Protoc 4, 102457.
[50] Öxler, E.-M., Dolga, A., Culmsee, C., 2012. AIF depletion provides neuroprotection through a preconditioning effect. Apoptosis 17, 1027–1038.
[51] Aguilar Diaz De Leon, J., Borges, C.R., 2020. Evaluation of oxidative stress in biological samples using the thiobarbituric acid reactive substances assay. J Vis Exp: JoVE.
[52] Yang, W.S., Stockwell, B.R., 2008. Synthetic lethal screening identifies compounds activating iron-dependent, nonapoptotic cell death in oncogenic-RAS-harboring cancer cells. Chem Biol 15, 234–245.
[53] Wang, D., Yin, K., Zhang, Y., Lu, H., Hou, L., Zhao, H., Xing, M., 2023. Fluoride induces neutrophil extracellular traps and aggravates brain inflammation by disrupting neutrophil calcium homeostasis and causing ferroptosis. Environ Pollut 331, 121847.
[54] Yuan, Y., Yucai, L., Lu, L., Hui, L., Yong, P., Haiyang, Y., 2022. Acrylamide induces ferroptosis in HSC-T6 cells by causing antioxidant imbalance of the XCT-GSH-GPX4 signaling and mitochondrial dysfunction. Toxicol Lett 368, 24–32.
[55] Liang, Z., Soriano-Castell, D., Kepchia, D., Duggan, B.M., Currais, A., Schubert, D., Maher, P., 2022. Cannabinol inhibits oxytosis/ferroptosis by directly targeting mitochondria independently of cannabinoid receptors. Free Radic Biol Med 180, 33–51.
[56] Fan, A., Liu, G., Wu, X., 2024. Nanosecond pulse electric field treatment initiates mitochondrial apoptosis pathway by inducing mitochondrial morphological changes in myocardial cells. J Interv Card Electrophysiol 1–8.
[57] Rochette, L., Dogon, G., Rigal, E., Zeller, M., Cottin, Y., Vergely, C., 2022. Lipid peroxidation and iron metabolism: two corner stones in the homeostasis control of ferroptosis. Int J Mol Sci 24, 449.
[58] Dai, Z., Zhang, W., Zhou, L., Huang, J., 2023. Probing lipid peroxidation in ferroptosis: emphasizing the utilization of C11-BODIPY-based protocols. In: Ferroptosis: Methods and Protocols. Springer, pp. 61–72.
[59] Mas-Bargues, C., Escriva, C., Dromant, M., Borras, C., Vina, J., 2021. Lipid peroxidation as measured by chromatographic determination of malondialdehyde. Human plasma reference values in health and disease. Arch Biochem Biophys 709, 108941.
[60] Costa, L.G., Cole, T.B., Dao, K., Chang, Y.-C., Coburn, J., Garrick, J.M., 2020. Effects of air pollution on the nervous system and its possible role in neurodevelopmental and neurodegenerative disorders. Pharmacol Ther 210, 107523.
[61] Gui, J., Liu, J., Han, Z., Yang, X., Ding, R., Yang, J., Luo, H., Huang, D., Chen, H., Cheng, L., 2023. The dysfunctionality of hippocampal synapses may be directly related to PM-induced impairments in spatial learning and memory in juvenile rats. Ecotoxicol Environ Saf 254, 114729.
[62] Milani, C., Farina, F., Botto, L., Lonati, E., Bulbarelli, A., Palestini, P., 2015. Oxidative stress and inflammation induced by diesel exhaust particles: pilot study in a model of neuronal cells. : N Perspect Neurosci: Res Results Young– Ital Neurosci.
[63] Cao, D., Bromberg, P.A., Samet, J.M., 2007. COX-2 expression induced by diesel particles involves chromatin modification and degradation of HDAC1. Am J Respir Cell Mol Biol 37, 232–239.
[64] Cattani-Cavalieri, I., Trombetta-Lima, M., Yan, H., Manzano-Covarrubias, A.L., Baarsma, H.A., Oun, A., van der Veen, M.M., Oosterhout, E., Dolga, A.M., Ostrom, R.S., 2024. Diesel exhaust particles alter mitochondrial bioenergetics and cAMP producing capacity in human bronchial epithelial cells. Front Toxicol 6.
[65] Vučković, A.M., Bosello Travain, V., Bordin, L., Cozza, G., Miotto, G., Rossetto, M., Toppo, S., Venerando, R., Zaccarin, M., Maiorino, M., 2020. Inactivation of the glutathione peroxidase GPx4 by the ferroptosis-inducing molecule RSL3 requires the adaptor protein 14-3-3ε. FEBS Lett 594, 611–624.
[66] Chen, T., Majerníková, Na, Marmolejo-Garza, A., Trombetta-Lima, M., Sabogal-Guáqueta, A.M., Zhang, Y., Ten Kate, R., Zuidema, M., Mulder, P.P., den Dunnen, W., 2023. Mitochondrial transplantation rescues neuronal cells from ferroptosis. Free Radic Biol Med 208, 62–72.
[67] Wang, X., Wang, Y., Huang, D., Shi, S., Pei, C., Wu, Y., Shen, Z., Wang, F., Wang, Z., 2022. Astragaloside IV regulates the ferroptosis signaling pathway via the Nrf2/SLC7A11/GPX4 axis to inhibit PM2. 5-mediated lung injury in mice. Int Immunopharmacol 112, 109186.
[68] Ma, Z., Du, X., Sun, Y., Jia, Y., Liang, X., Gao, Y., 2024. Attenuation of PM2. 5-induced lung injury by 4-phenylbutyric acid: maintenance of [Ca2+] i stability between endoplasmic reticulum and mitochondria. Biomolecules 14, 1135.
[69] Zhu, S., Li, X., Dang, B., Wu, F., Wang, C., Lin, C., 2022. Lycium barbarum polysaccharide protects HaCaT cells from PM2. 5-induced apoptosis via inhibiting oxidative stress, ER stress and autophagy. Redox Rep 27, 32–44.
[70] Shin, T.H., Kim, S.G., Ji, M., Kwon, D.H., Hwang, J.S., George, N.P., Ergando, D.S., Park, C.B., Paik, M.J., Lee, G., 2022. Diesel-derived PM2. 5 induces impairment of cardiac movement followed by mitochondria dysfunction in cardiomyocytes. Front Endocrinol 13, 999475.
[71] Gu, L., Larson-Casey, J.L., Carter, A.B., 2017. Macrophages utilize the mitochondrial calcium uniporter for profibrotic polarization. FASEB J 31, 3072.
[72] Lim, D., Dematteis, G., Tapella, L., Genazzani, A.A., Calì, T., Brini, M., Verkhratsky, A., 2021. Ca2+ handling at the mitochondria-ER contact sites in neurodegeneration. Cell Calcium 98, 102453.
[73] Xu, L., Wang, X., Tong, C., 2020. Endoplasmic reticulum–mitochondria contact sites and neurodegeneration. Front Cell Dev Biol 8, 428.
[74] Chang-Chien, J., Huang, J.-L., Tsai, H.-J., Wang, S.-L., Kuo, M.-L., Yao, T.-C., 2024. Vitamin D ameliorates particulate matter induced mitochondrial damages and calcium dyshomeostasis in BEAS-2B human bronchial epithelial cells. Respir Res 25, 321.
[75] Piao, M.J., Kang, K.A., Zhen, A.X., Fernando, P.D.S.M., Ahn, M.J., Koh, Y.S., Kang, H.K., Yi, J.M., Choi, Y.H., Hyun, J.W., 2019. Particulate matter 2.5 mediates cutaneous cellular injury by inducing mitochondria-associated endoplasmic reticulum stress: protective effects of ginsenoside Rb1. Antioxidants 8, 383.
[76] Liu, B., Han, Y., Ye, Y., Wei, X., Li, G., Jiang, W., 2024. Atmospheric fine particulate matter (PM2. 5) induces pulmonary fibrosis by regulating different cell fates via autophagy. Sci Total Environ 923, 171396.
[77] Wang, B., Wang, Y., Zhang, J., Hu, C., Jiang, J., Li, Y., Peng, Z., 2023. ROS-induced lipid peroxidation modulates cell death outcome: mechanisms behind apoptosis, autophagy, and ferroptosis. Arch Toxicol 97, 1439–1451.
[78] Majerníková, N., Marmolejo-Garza, A., Salinas, C.S., Luu, M.D., Zhang, Y., Trombetta-Lima, M., Tomin, T., Birner-Gruenberger, R., Lehtonen, Š., Koistinaho, J., 2024. The link between amyloid β and ferroptosis pathway in Alzheimer's disease progression. Cell Death Dis 15, 782.
[79] Guo, C.C., Xu, Z.M., Lyu, Y., Li, X.H., Li, Z.F., He, H., Tian, F.J., Zheng, J.P., 2023. PM2. 5 induces autophagy-dependent ferroptosis by endoplasmic reticulum stress in SH-SY5Y cells. J Appl Toxicol 43, 1013–1025.
[80] Mutlu, E.A., Engen, P.A., Soberanes, S., Urich, D., Forsyth, C.B., Nigdelioglu, R., Chiarella, S.E., Radigan, K.A., Gonzalez, A., Jakate, S., 2011. Particulate matter air pollution causes oxidant-mediated increase in gut permeability in mice. Part Fibre Toxicol 8, 1–13.

[81] Trombetta-Lima, M., Sabogal-Guáqueta, A.M., Dolga, A.M., 2021 Mar. Mitochondrial dysfunction in neurodegenerative diseases: a focus on iPSC-derived neuronal models. Cell Calcium 94, 102362.
[82] Sabogal-Guáqueta, A.M., Marmolejo-Garza, A., Trombetta-Lima, M., Oun, A., Hunneman, J., Chen, T., Koistinaho, J., Lehtonen, S., Kortholt, A., Wolters, J.C., Bakker, B.M., Eggen, B.J.L., Boddeke, E., Dolga, A., 2023 Oct 13. Species-specific metabolic reprogramming in human and mouse microglia during inflammatory pathway induction. Nat Commun 14 (1), 6454.
[83] Sabogal-Guaqueta, A.M., Mitchell-Garcia, T., Hunneman, J., Voshart, D., Thiruvalluvan, A., Foijer, F., Kruyt, F., Trombetta-Lima, M., Eggen, B.J.L., Boddeke, E., Barazzuol, L., Dolga, A.M., 2024 Dec. Brain organoid models for studying the function of iPSC-derived microglia in neurodegeneration and brain tumours. Neurobiol Dis 203, 106742.